General Disclaimer

One or more of the Following Statements may affect this Document

- This document has been reproduced from the best copy furnished by the organizational source. It is being released in the interest of making available as much information as possible.

- This document may contain data, which exceeds the sheet parameters. It was furnished in this condition by the organizational source and is the best copy available.

- This document may contain tone-on-tone or color graphs, charts and/or pictures, which have been reproduced in black and white.

- This document is paginated as submitted by the original source.

- Portions of this document are not fully legible due to the historical nature of some of the material. However, it is the best reproduction available from the original submission.

UPPER ATMOSPHERE DYNAMICS

M. P. FRIEDMAN

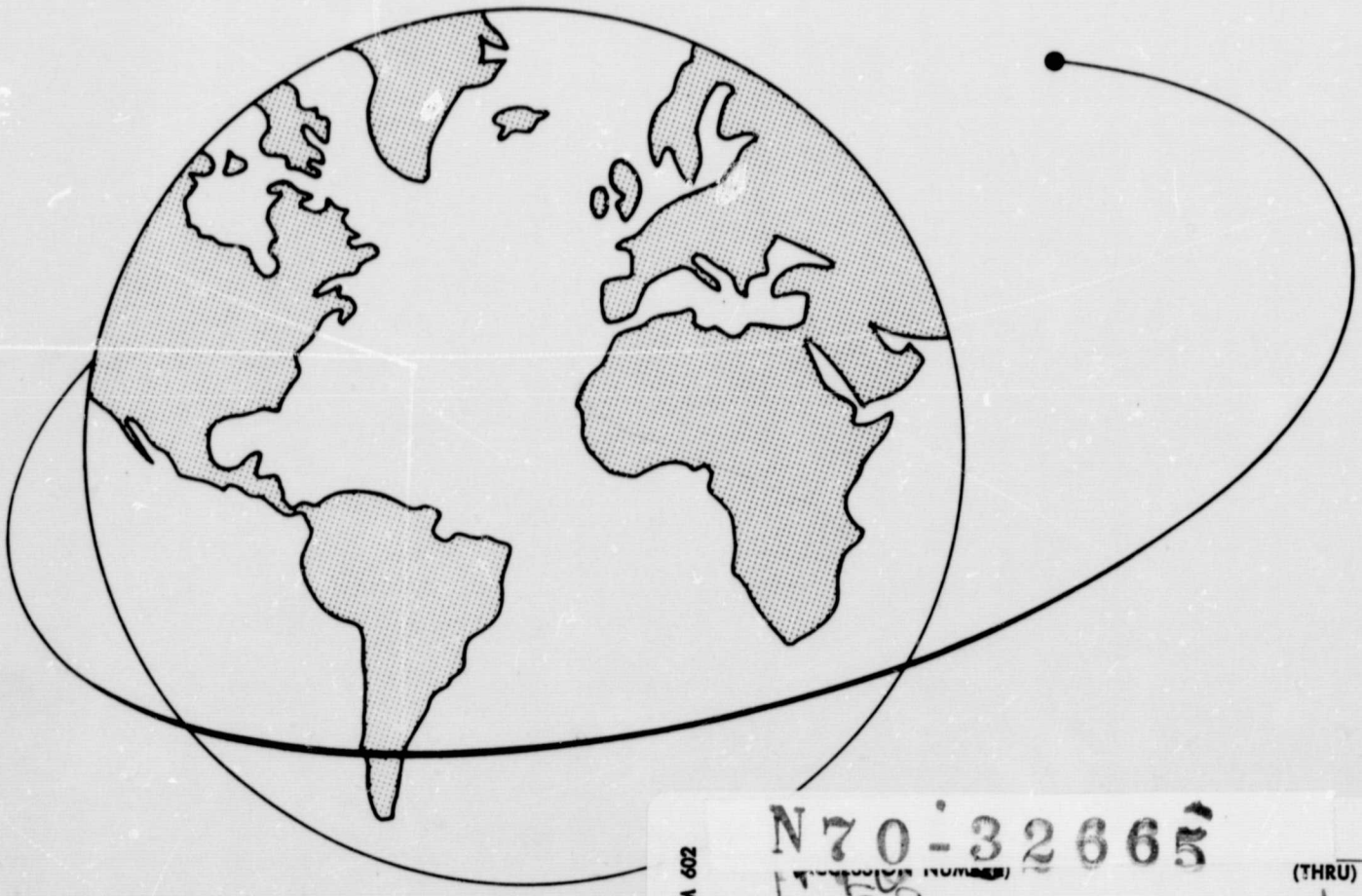

Smithsonian Astrophysical Observatory
SPECIAL REPORT 316

Research in Space Science
SAO Special Report No. 316

UPPER ATMOSPHERE DYNAMICS

Manfred P. Friedman

May 28, 1970

Smithsonian Institution
Astrophysical Observatory
Cambridge, Massachusetts 02138

TABLE OF CONTENTS

LIST OF ILLUSTRATIONS

LIST OF TABLES

ABSTRACT

We are able to construct three-dimensional global models of the upper atmosphere (120 to 800 km) by solving the conservation equations of mass, momentum, and energy. We show that variation of conditions at the lower boundary, 120 km, affects the atmosphere only to about 200-km altitude. Differing results obtained by in situ satellite or rocket measurements in the 120- to 200-km range can therefore be explained as resulting from atmospheric behavior below 120 km.

We report on a study of possible wind fields and find diurnally varying winds with no steady east-to-west flow. Viscous forces at the higher altitudes match the pressure gradient forces and give rise to small wind magnitudes above 300 km. Maximum wind speeds are found to occur near 140 km, where viscous effects are not too great.

RÉSUMÉ

La résolution des équations de conservation de la masse, de la quantité de mouvement et de l'énergie nous permet de construire des modèles globaux, à trois dimensions, de la haute atmosphère (120 à 800 km). Nous montrons qu'une variation des conditions au plus bas niveau, 120 km, affecte l'atmosphère jusqu'à une altitude de 200 km seulement. On peut donc expliquer les résultats discordants fournis par les mesures effectuées par satellites in situ ou par fusées, dans la région allant de 120 à 200 km, comme étant dûs au comportement de l'atmosphère en dessous de 120 km.

Nous donnons le compte-rendu d'une étude de champs de vents possibles et trouvons des vents variant journellement sans courant régulier est-ouest. Aux plus hautes altitudes, les forces de viscosité égalisent les forces du gradient de pression et donnent naissance à de faibles vents au-dessus de 300 km. On trouve que les vents sont les plus forts près de 140 km, où les effets de la viscosité ne sont pas trop grands.

КОНСПЕКТ

Решая уравнение сохранения массы, момента сил и энергии, мы в состоянии построить трехмерные шаровые модели верхних слоев атмосферы (120-800 км). Мы показываем, что изменение условий на нижней границе - 120 км, оказывает влияние на атмосферные слои в пределах лишь 200 км высоты. Отличающиеся результаты, полученные при помощи космических полетов, для высот 120-200 км могут быть объяснены за счет атмосферного состояния ниже 120 км.

Мы занимались вопросом изучения возможных ветровых полей и обнаружили суточно переменные ветры, не имеющие постоянного направления ветра с востока на запад. Силы вязкости высоких слоев совпадают с градиентом силы давления и способствуют увеличению слабых ветров выше 300 км. Как было обнаружено, максимальная скорость ветра достигается на высоте приблизительно 140 км, где силы вязкости не очень велики.

UPPER ATMOSPHERE DYNAMICS

Manfred P. Friedman

1. INTRODUCTION

This paper describes a continuation of work presented in SAO Special Report No. 250, "A Three-Dimensional Model of the Upper Atmosphere" (Friedman, 1967). The work is based on our ability to construct by theoretical means three-dimensional global models of the upper atmosphere. We do this by numerically solving the partial differential equations of conservation of mass, momentum, and energy in a spherical coordinate system and between the altitudes 120 and 800 km. The densities of O_2, N_2, O, He, and H, as well as temperature and winds, can be computed, and the main input to the problem is solar EUV (extreme ultraviolet) radiational heating.

We do not consider chemical dissociation or recombination interactions. In addition, the present state of knowledge prevents us from giving too accurate a description of the energy input. Our model of the solar heating process, as well as other details of the formulation, is described in Friedman (1967).

Two major improvements to our previous paper have been made. The first is mathematical: by changing to a larger computer (CDC 6400) we were able to decrease the spacing between altitudes. We now have a mesh of 69 altitudes, compared with the 40 used earlier. Also, the vertical spacing is now at most 1/4 scale height.

The second improvement is in the physical formulation. In the earlier work, we neglected winds and assumed that the atmosphere rotates essentially as a rigid body with the earth. This formulation simplified the

This work was supported in part by grant NGR 09-015-002 from the National Aeronautics and Space Administration.

analysis yet permitted us to predict the major features of the upper atmosphere. We were able to ascertain, for example, that the daytime bulge migrates with the subsolar point, north and south of the equator, during seasonal changes. We know, from the fact that pressure gradients exist, there must be bulk motions within the atmosphere. In order to determine the importance of these motions, we have extended the previous analysis to include winds. Our present formulation is capable of computing winds as well as temperature and density on a global scale.

In Section 2 we present our basic equations and give a brief description of their derivation. Our results of computing an atmosphere without winds but with different boundary conditions are discussed in Section 3. We find that the atmosphere above 200 km is insensitive to changes in conditions at 120 km. In Section 4 we describe the results of our computations involving winds. Our main finding is that the winds attain their maximum magnitude near 140 km and that above 140 km they decrease in magnitude with increasing altitude.

2. COORDINATE SYSTEM AND EQUATIONS

2.1 Coordinate System

Before we give the basic equations, it will be helpful to describe the coordinate system (Figure 1). We use a spherical coordinate system where the origin is at the earth's center and the polar axis coincides with the earth's axis of rotation. For numerical treatment we use a mesh consisting of 69 (unequally spaced) altitudes between 120 and 800 km, 12 longitudes (30° spacing), and 9 latitudes (22.5 spacing). The sun is stationary and the earth rotates with respect to the coordinate system; for this reason, it is sometimes convenient to use the appellation local solar time (LST) rather than longitude. The longitudinal spacing, then, is every 2 hours.

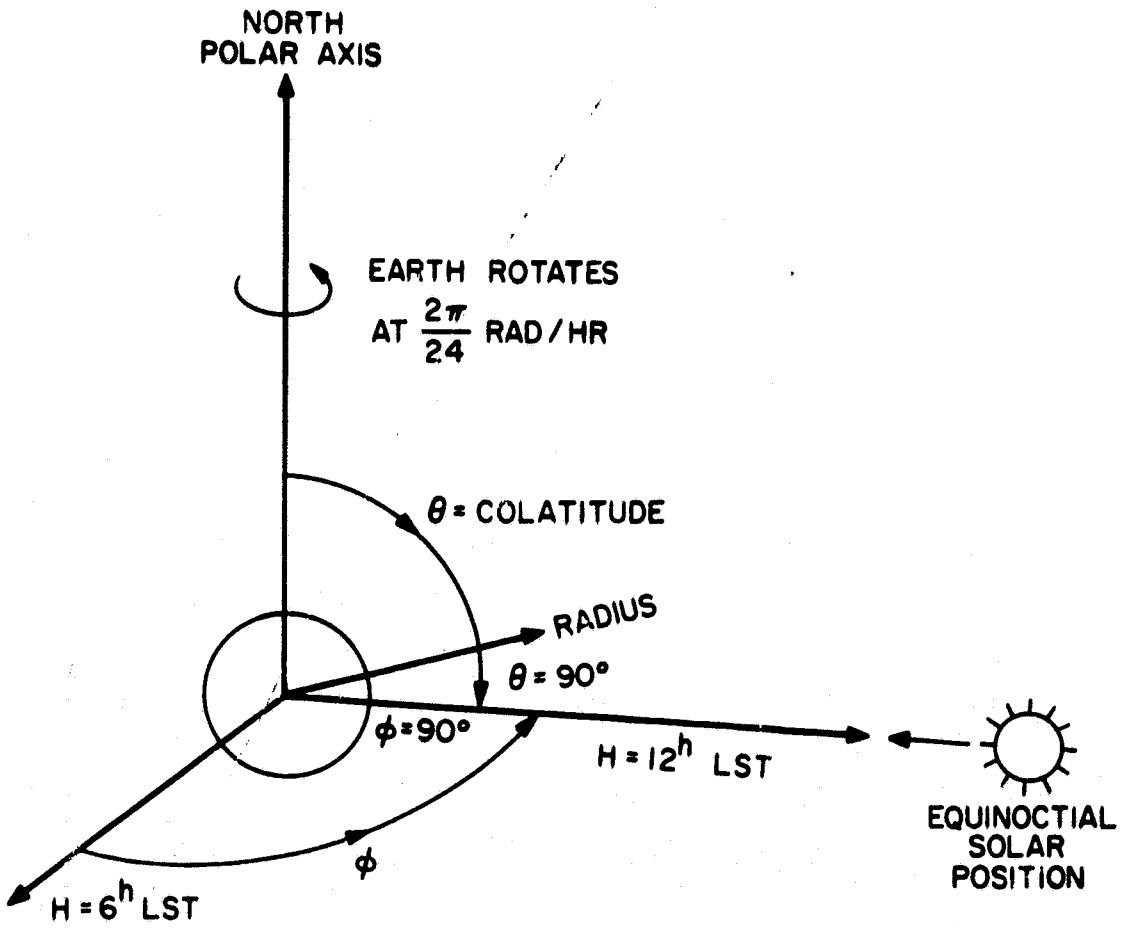

Figure 1. Coordinate system used for computations. The system is fixed at the center of the earth and contains the sun; the earth rotates with respect to the system: θ = colatitude, ϕ = hour angle.

We are interested in determining the state of the atmosphere corresponding to given temperature and density data at 120 km and solar heating on the sunlit part of the atmosphere. Studies of satellite-drag data (Jacchia, 1965) have shown periodic variations of 24-hour, 24-day, semiannual, and 11-year durations as well as transient changes that correspond to solar and/or geomagnetic activity. If we were to have a formulation general enough to include all these effects, we would need as independent variables time and three space coordinates. However, solution of problems with four independent variables would take an inordinately large amount of computer time. We therefore compromise by solving only for the 24-hour or diurnal atmospheric behavior. This is done in a most natural way with our global coordinate system by simply assuming no time dependence. We determine an equilibrium solution that encompasses both the sunlit side and the night side, and our independent variables are the three space coordinates of latitude, hour (longitude), and altitude. The reduction from four to three independent variables has brought the problem to an almost manageable formulation.

After a given set of input parameters has been prescribed, it takes about an hour of computing time for the atmosphere to come to a final equilibrium state; of course, this time depends on how near the initial atmosphere is to the final atmosphere. However, once we have attained a solution, we have the equivalent of 84 one-dimensional solutions all in diurnal equilibrium. The number 84 comes from 7 latitudes and 12 hours; the remaining 2 latitudes are the north and south poles, which are singular points for our spherical coordinate system (we do not solve the conservation equations at these points).

2.2 Equations of Mass, Momentum, and Energy Conservation

Details of the derivation of these equations are given by Friedman (1967); the only change is that we include winds in the present equations. We will therefore omit a lengthy derivation and present only the initial equations, a definition of terms, and the final results. We are dealing with a multicomponent gas mixture, and our starting equations are derived from basic principles in Chapman and Cowling (1960) and Hirschfelder, Curtiss, and Bird (1964).

2.2.1 Number-density conservation

We assume that there is no creation or loss of constituents through chemical means; therefore, we start with

$$\frac{\partial n_i}{\partial t} + \nabla \cdot (n_i \vec{v}) + \nabla \cdot (n_i \vec{V}_i) = 0 \quad , \tag{1}$$

where

n_i = number density of ith species (i = 1, 2, 3, 4, 5) corresponding to O_2, N_2, O, He, and H, respectively,

$\vec{v}$ = macroscopic velocity,

$\vec{V}_i$ = diffusion velocity of ith species.

The macroscopic velocity, i. e., wind, is given by

$$\vec{v} = (w_r, w_\theta, w_\phi) = [0, r\omega v_\theta, r\omega(\sin\theta + v_\phi)] \quad , \tag{2}$$

where

r = radius from center of the earth,

θ = colatitude,

ϕ = hour angle,

ω = earth rotation rate = 7.27×10^{-5} rad/sec,

w = dimensional wind component,

v = dimensionless wind component.

We neglect vertical winds and consider only the horizontal winds v_θ and v_ϕ, which have been made dimensionless by the factor $r\omega$. The quantity $r\omega \sin\theta$ is the earth's rotation velocity at altitude r and colatitude θ; since the earth rotates relative to the coordinate system (Figure 1), this quantity must be included in the velocity definition. The meridional wind v_θ is positive when it is from north to south; the zonal wind v_ϕ is positive from west to east.

The diffusion velocity is

$$\vec{V}_i = - D_i \left[\frac{\nabla n_i}{n_i} + \left(1 + \alpha_{T_i}\right) \frac{\nabla T}{T} - \frac{M_i}{kT\rho} \nabla p \right] \quad , \qquad (3)$$

where

D_i = diffusion coefficient,

α_{T_i} = thermal diffusion coefficient,

M_i = molecular mass, ith constituent,

k = Boltzmann constant,

ρ = density,

p = pressure.

We combine equations (1) and (2), recalling that our steady-state diurnal solution is independent of time, to get

$$\frac{\omega}{\sin\theta} \left[\frac{\partial}{\partial\theta} (n_i v_\theta \sin\theta) + \frac{\partial}{\partial\phi} n_i (\sin\theta + v_\phi) \right] + \nabla \cdot n_i V_i = 0 \quad . \qquad (4)$$

2.2.2 Energy conservation equation

The energy equation is derived in Appendix A of Friedman (1967); we need only add a term that describes energy losses due to viscous shear:

$$\rho C_p \frac{DT}{Dt} - \frac{Dp}{Dt} = \nabla \cdot \lambda \nabla T - \sum \rho_i C_{p_i} \vec{V}_i \cdot \nabla T + \tau_{ij} : \nabla \vec{v} + Q \quad , \qquad (5)$$

where

C_p = specific heat at constant pressure,

T = temperature,

$$\frac{D}{Dt} = \frac{\partial}{\partial t} + w_r \frac{\partial}{\partial r} + \frac{w_\theta}{r} \frac{\partial}{\partial\theta} + \frac{w_\phi}{r \sin\theta} \frac{\partial}{\partial\phi} \quad ,$$

τ_{ij} = shear stress tensor,

Q = external energy-source term.

The third term on the right side of equation (5) is the viscous shear contribution. The shear stress tensor τ_{ij} is quite lengthy when expressed in spherical coordinates and will not be reproduced here. The inquisitive reader may find it written out in Bird, Stewart, and Lightfoot (1966, p. 91). If we use velocities as defined in equation (2) and neglect earth curvature, $1/r \ll \partial/\partial r$, we can approximate the viscous friction term as

$$\tau_{ij} : \vec{\nabla v} = \mu \left[\left(\frac{\partial w_\theta}{\partial r} \right)^2 + \left(\frac{\partial w_\phi}{\partial r} \right)^2 \right] , \qquad (6)$$

where μ = viscosity coefficient.

The energy equation, in its final form, is

$$\omega \rho C_p \left[v_\theta \frac{\partial T}{\partial \theta} + \left(1 + \frac{v_\phi}{\sin \theta} \right) \frac{\partial T}{\partial \phi} \right] - \omega \left[v_\theta \frac{\partial p}{\partial \theta} + \left(1 + \frac{v_\phi}{\sin \theta} \right) \frac{\partial p}{\partial \phi} \right]$$

$$= \nabla \cdot \lambda \nabla T - \sum \rho_i C_{p_i} \vec{V}_i \cdot \nabla T + \mu r^2 \omega^2 \left[\left(\frac{\partial v_\theta}{\partial r} \right)^2 + \left(\frac{\partial v_\phi}{\partial r} \right)^2 \right] + Q . \qquad (7)$$

2.2.3 Momentum conservation equation

Again, for brevity, we will not write out the full momentum equations — with viscous shear terms — in spherical coordinates. These can be found in Bird et al. (1966, pp. 86 and 90). In order to arrive at their final form, we have assumed that

A. Horizontal logarithmic derivatives of viscosity are negligible: $|\partial \ell n \mu / \partial \phi|$ or $|\partial \ell n \mu / \partial \theta| \ll 1$.

B. Terms arising from earth curvature are negligible relative to radial derivatives: $1/r \ll \partial/\partial r$.

C. Horizontal shear terms are negligible with respect to vertical shear terms: $(1/r)\,(\partial/\partial\phi)$ or $(1/r)\,(\partial/\partial\theta) << \partial/\partial r$.

D. Nonlinear momentum transport terms have been retained.

The momentum equations are

$$v_\theta^2 + (\sin\theta + v_\phi)^2 = \frac{1}{\rho r\omega^2}\ \frac{\partial p}{\partial r} + \frac{GM_0}{r^3\omega^2} - \frac{\mu}{3r\rho\omega\sin\theta}$$

$$\times \frac{\partial}{\partial r}\left(\frac{\partial}{\partial\theta}\ v_\theta \sin\theta + \frac{\partial v_\phi}{\partial\phi}\right) \quad , \tag{8}$$

$$v_\theta\ \frac{\partial v_\theta}{\partial\theta} + \left(1 + \frac{v_\phi}{\sin\theta}\right)\ \frac{\partial v_\theta}{\partial\phi} - \left(1 + \frac{v_\phi}{\sin\theta}\right)^2 \sin\theta\cos\theta$$

$$= \frac{-1}{\rho r^2\omega^2}\ \frac{\partial p}{\partial\theta} + \frac{1}{\rho\omega}\ \frac{\partial}{\partial r}\left(\mu\ \frac{\partial v_\theta}{\partial r}\right) \quad , \tag{9}$$

and

$$v_\theta\ \frac{\partial v_\phi}{\partial\theta} + \left(1 + \frac{v_\phi}{\sin\theta}\right)\frac{\partial v_\phi}{\partial\phi} + 2v_\theta\cos\theta + v_\theta v_\phi\cot\theta = \frac{-1}{\rho r^2\omega^2\sin\theta}\ \frac{\partial p}{\partial\phi}$$

$$+ \frac{1}{\rho\omega}\ \frac{\partial}{\partial r}\left(\mu\ \frac{\partial v_\phi}{\partial r}\right) \quad , \tag{10}$$

where

GM_0 = gravitational constant multiplied by earth mass
$= 4 \times 10^5\ km^3/sec^2$,

v_θ, v_ϕ = dimensionless meridional zonal wind speed defined in equation (2).

Since we are neglecting vertical velocities, equation (8) is redundant and horizontal velocities are determined by solving equations (9) and (10).

2.2.4 Viscosity and thermal conductivity coefficients

The upper atmosphere in the altitude range we are considering is not a homogeneous gas mixture, since its constituent composition is everywhere changing. Because of this, expressions for the transport coefficients are quite complex; their derivation is discussed in Hirschfelder et al. (1964, chapters 7 and 8). However, it is possible to approximate them with sufficient accuracy by use of formulas given in Bird et al. (1966, pp. 24 and 258):

viscosity coefficient:

$$\mu_{mix} = \sum_i \frac{n_i \mu_i}{\sum_j n_j \Phi_{ij}} \quad ;$$

thermal conductivity coefficient:

$$\lambda_{mix} = \sum_i \frac{n_i \lambda_i}{\sum_j n_j \Phi_{ij}} \quad ,$$

where

$$\Phi_{ij} = \left(\frac{\sigma_i + \sigma_j}{2\sigma_i} \right)^2 \sqrt{\frac{2 M_j}{M_i + M_j}} \quad ,$$

σ_i = atomic collision cross section of ith constituent,

M_i = molecular mass, ith constituent,

$$\mu_i = \frac{5}{16 \sigma_i^2} \sqrt{\frac{M_i k T}{\pi}} \quad ,$$

$$\lambda_i = \frac{75k}{64 \sigma_i^2} \sqrt{\frac{k T}{\pi M_i}} \quad .$$

All summations are over the five constituents O_2, N_2, O, He, and H.

3. RESULTS OF MODEL-ATMOSPHERE CALCULATIONS

Our three-dimensional model and method of analysis permit us to carry out atmosphere determinations that are quite general: we are able simultaneously to determine density, temperature, and winds. This is especially important for wind calculations, since earlier authors (Geisler, 1966, 1967; Kohl and King, 1967; Challinor, 1968, 1969) computed winds using a fixed atmospheric background, and the effects of the computed winds on the temperature and density distributions were not determined.

3.1 Problems Considered

We have set out a program to determine the effect of winds in the following manner: First, we compute an atmosphere without winds. Next, we use this equilibrium atmosphere as a background for a wind computation; that is, as in the references mentioned above, we compute winds without calculating their effect on the atmosphere. We do this quite simply by solving only the momentum equation, bypassing the mass and energy equations. Finally, we start over and compute an atmosphere using the full set of conservation equations and simultaneously determine temperature, density, and wind.

3.2 Temperature and Density Computations without Winds

We have run several experiments without winds to determine the effect of an improved numerical formulation as well as to study the effect of different boundary conditions at the base of our atmosphere, 120 km.

We computed the earlier results (Friedman, 1967) using a 40-altitude mesh between 120 and 800 km; for the present results we use 69 altitudes. With this number of altitudes we are able to adjust the mesh spacing to at

most 1/4 scale height throughout. Hence, computations are more stable and converge more quickly; however, because of the additional altitudes, more computing is required. The net result is a trade off, and the overall computation time between an initial and a final atmosphere remains about the same, roughly 60 to 90 min on the CDC 6400. What we have gained are greater accuracy and more confidence in our final result.

3.2.1 Boundary-condition effects

The present computed atmosphere corresponds to a higher exospheric temperature than that of the earlier one (Friedman, 1967); we generate this atmosphere by increasing the magnitude of the solar EUV heating. Two or three years ago the general feeling was that atmospheric conditions at 120 km remained constant. We therefore started with the same boundary conditions at 120 km as were used in our previous work. This was found to be incompatible with the increased heating. At the lowest altitudes (below 160 km), where the scale height is smallest and hence the numerical sensitivity is greatest, we found that the gradients between our 120-km fixed data and our computed data near 160 km were too large.

The altitude of maximum solar EUV absorption is near 150 km. This apparently caused excessive heating with respect to our fixed conditions at 120 km; calculations would not converge. After adjusting the temperatures and densities at 120 km to higher values we obtained convergence.

This result gives support to recent (Jacchia, 1969) findings: measured diurnal density variations at 160 km are inconsistent with a constant atmosphere at 120 km; hence, the level of constant diurnal temperature and density (if one exists) must be lowered to an altitude probably below 100 km.

Figure 2 shows the effects of three different boundary conditions on the computed atmosphere at several altitudes between 120 and 240 km. In addition, we give, for comparison, data obtained from Jacchia's most recent model (1969, private communication). Equatorial density profiles are plotted against local time of day.

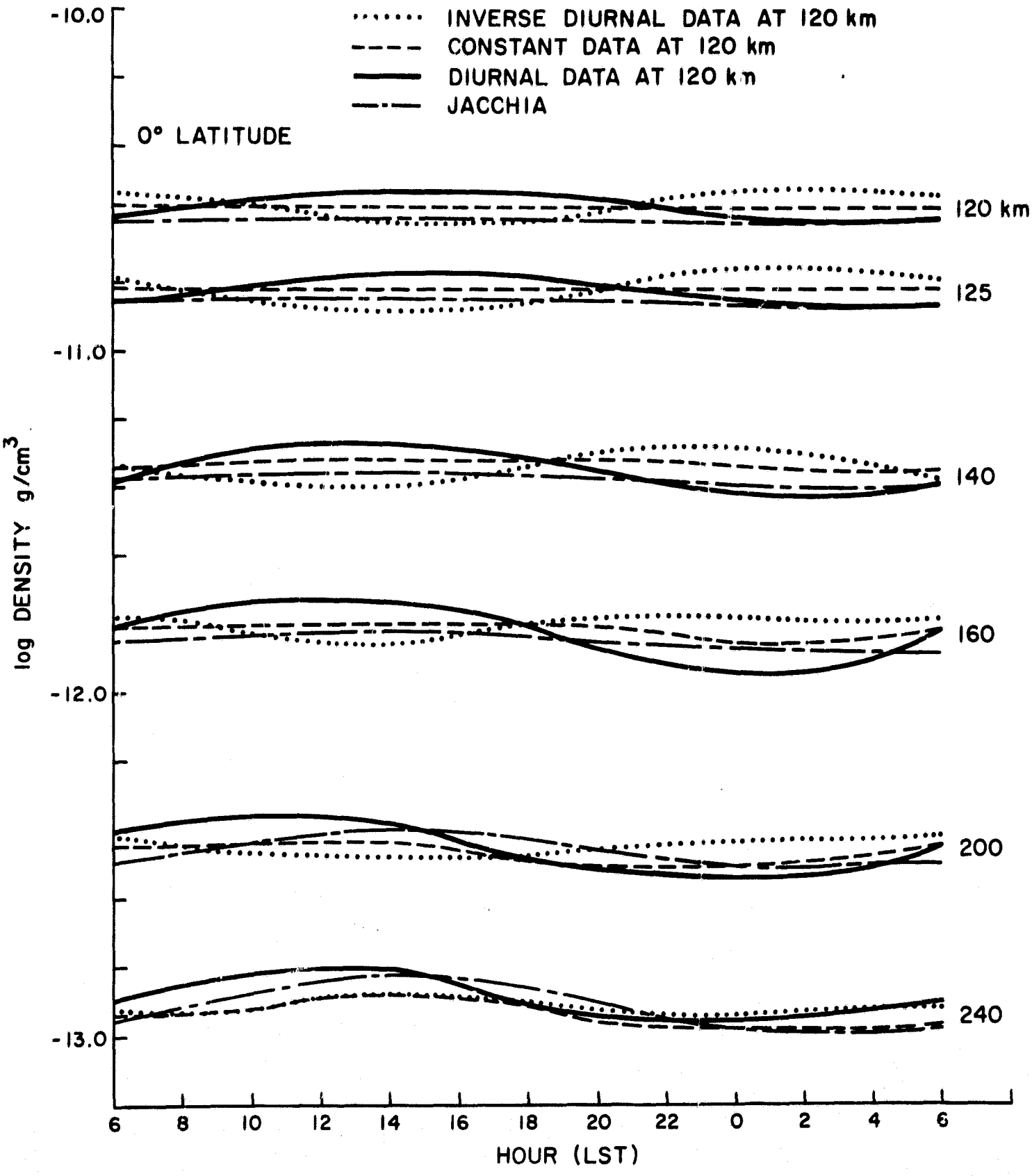

Figure 2. The effect of different boundary conditions at 120 km on diurnal equatorial density profiles for altitudes between 120 and 240 km.

The three boundary conditions set at 120 km are diurnally varying temperature and density with a maximum near 15^h and a minimum near 4^h; constant temperature and density; and inverse diurnal temperature and density with maximum and minimum near 2^h and 16^h, respectively. There is also a latitudinal variation of the boundary data for the first and third cases; the second case is constant throughout. In lieu of lengthy descriptions, these boundary data are listed in Tables 1, 2, and 3, respectively.

Results at these low altitudes clearly reflect the boundary conditions; for example, the case with inverse sinusoidal data at 120 km shows that this behavior persists to about 200-km altitude. Above 240 km, the effect of the lower boundary condition rapidly becomes negligible and all three problems give indistinguishable results.

These low-altitude results, varying with boundary conditions, are quite interesting in light of some recent atmospheric measurements in the vicinity of 150 km. King-Hele and Hingston (1967), by reducing satellite-drag data, find a strong diurnal atmospheric structure near 150 km, i. e., a diurnal density variation by a factor of 1. 7. Although this variation may have been exaggerated by their neglect of the semiannual variation (Jacchia, 1969), there must certainly have been more structure than exhibited by existing (CIRA, 1965; Jacchia, 1965) atmospheric models. On the other hand, after evaluating data from another low-altitude satellite, King-Hele and Walker (1969) find very little diurnal variation. Weidner and Swenson (1969), measuring nitrogen densities with mass-spectrometer probes, find a relatively flat density profile from $10^h.0$ to $22^h.0$ and a small drop in density during early morning hours. Furthermore, they find that the familiar diurnal density profile does not develop until the 200-km altitude is reached.

It is our opinion that these different readings of atmospheric behavior are all valid and are only a reflection of "weather" near the 100-km level. Since the solar EUV energy is deposited mainly at the 150-km level, this source helps obliterate lower level phenomena and sets up the basic diurnal nature of the upper atmosphere. Atmospheric behavior between 100 and 200 km, especially between 100 and 150 km, where problems of turbulence

Table 1. Diurnally varying boundary data at 120 km. These temperatures and densities vary both diurnally and latitudinally so as to have a daytime maximum and a nighttime minimum at the equator.

	LOCAL SOLAR TIME											
LATITUDE	6	8	10	12	14	16	18	20	22	24	2	4
90.0	372.5 -10.5678	374.7 -10.5678	377.0 -10.5678	374.7 -10.5678	372.5 -10.5678	370.6 -10.5678	369.2 -10.5678	368.3 -10.5678	368.0 -10.5678	368.3 -10.5678	369.2 -10.5678	370.6 -10.5678
67.5	368.9 -10.5851	372.6 -10.5721	377.0 -10.5561	376.8 -10.5525	376.1 -10.5512	374.8 -10.5534	372.9 -10.5596	370.4 -10.5688	368.0 -10.5792	366.2 -10.5883	365.6 -10.5934	366.4 -10.5926
45.0	365.8 -10.6003	370.8 -10.5806	377.0 -10.5561	378.6 -10.5445	379.2 -10.5376	378.4 -10.5378	375.9 -10.5459	372.2 -10.5607	368.0 -10.5792	364.4 -10.5969	362.5 -10.6086	362.9 -10.6103
22.5	363.7 -10.6107	369.6 -10.5864	377.0 -10.5561	379.8 -10.5392	381.3 -10.5287	380.8 -10.5277	378.0 -10.5371	373.4 -10.5554	368.0 -10.5792	363.2 -10.6027	360.4 -10.6191	360.5 -10.6225
0.0	363.0 -10.6145	369.2 -10.5885	377.0 -10.5561	380.2 -10.5373	382.0 -10.5256	381.6 -10.5242	378.7 -10.5340	373.8 -10.5536	368.0 -10.5792	362.8 -10.6048	359.7 -10.6228	359.6 -10.6269
-22.5	363.7 -10.6107	369.6 -10.5864	377.0 -10.5561	379.8 -10.5392	381.3 -10.5287	380.8 -10.5277	378.0 -10.5371	373.4 -10.5554	368.0 -10.5792	363.2 -10.6027	360.4 -10.6191	360.5 -10.6225
-45.0	365.8 -10.6003	370.8 -10.5806	377.0 -10.5561	378.6 -10.5445	379.2 -10.5376	378.4 -10.5378	375.9 -10.5459	372.2 -10.5607	368.0 -10.5792	364.4 -10.5969	362.5 -10.6086	362.9 -10.6103
-67.5	368.9 -10.5851	372.6 -10.5721	377.0 -10.5561	376.8 -10.5525	376.1 -10.5512	374.8 -10.5534	372.9 -10.5596	370.4 -10.5688	368.0 -10.5792	366.2 -10.5883	365.6 -10.5934	366.4 -10.5926
-90.0	372.5 -10.5678	374.7 -10.5678	377.0 -10.5678	374.7 -10.5678	372.5 -10.5678	370.6 -10.5678	369.2 -10.5678	368.3 -10.5678	368.0 -10.5678	368.3 -10.5678	369.2 -10.5678	370.6 -10.5678

Table 2. Constant boundary data at 120 km. Temperature and density are assumed to be uniformly constant at 120-km altitude.

	LOCAL SOLAR TIME											
LATITUDE	6	8	10	12	14	16	18	20	22	24	2	4
90.0	371.3 -10.5707	371.3 -10.5707	371.3 -10.5707	371.3 -10.5707	371.3 -10.5707	371.3 -10.5707	371.3 -10.5707	371.3 -10.5707	371.3 -10.5707	371.3 -10.5707	371.3 -10.5707	371.3 -10.5707
67.5	371.3 -10.5707	371.3 -10.5707	371.3 -10.5707	371.3 -10.5707	371.3 -10.5707	371.3 -10.5707	371.3 -10.5707	371.3 -10.5707	371.3 -10.5707	371.3 -10.5707	371.3 -10.5707	371.3 -10.5707
45.0	371.3 -10.5707	371.3 -10.5707	371.3 -10.5707	371.3 -10.5707	371.3 -10.5707	371.3 -10.5707	371.3 -10.5707	371.3 -10.5707	371.3 -10.5707	371.3 -10.5707	371.3 -10.5707	371.3 -10.5707
22.5	371.3 -10.5707	371.3 -10.5707	371.3 -10.5707	371.3 -10.5707	371.3 -10.5707	371.3 -10.5707	371.3 -10.5707	371.3 -10.5707	371.3 -10.5707	371.3 -10.5707	371.3 -10.5707	371.3 -10.5707
0.0	371.3 -10.5707	371.3 -10.5707	371.3 -10.5707	371.3 -10.5707	371.3 -10.5707	371.3 -10.5707	371.3 -10.5707	371.3 -10.5707	371.3 -10.5707	371.3 -10.5707	371.3 -10.5707	371.3 -10.5707
-22.5	371.3 -10.5707	371.3 -10.5707	371.3 -10.5707	371.3 -10.5707	371.3 -10.5707	371.3 -10.5707	371.3 -10.5707	371.3 -10.5707	371.3 -10.5707	371.3 -10.5707	371.3 -10.5707	371.3 -10.5707
-45.0	371.3 -10.5707	371.3 -10.5707	371.3 -10.5707	371.3 -10.5707	371.3 -10.5707	371.3 -10.5707	371.3 -10.5707	371.3 -10.5707	371.3 -10.5707	371.3 -10.5707	371.3 -10.5707	371.3 -10.5707
-67.5	371.3 -10.5707	371.3 -10.5707	371.3 -10.5707	371.3 -10.5707	371.3 -10.5707	371.3 -10.5707	371.3 -10.5707	371.3 -10.5707	371.3 -10.5707	371.3 -10.5707	371.3 -10.5707	371.3 -10.5707
-90.0	371.3 -10.5707	371.3 -10.5707	371.3 -10.5707	371.3 -10.5707	371.3 -10.5707	371.3 -10.5707	371.3 -10.5707	371.3 -10.5707	371.3 -10.5707	371.3 -10.5707	371.3 -10.5707	371.3 -10.5707

Table 3. Inverse diurnally varying boundary data at 120 km. These temperatures and densities are adjusted so as to have a nighttime maximum and a daytime minimum at the equator.

	LOCAL SOLAR TIME											
LATITUDE	6	8	10	12	14	16	18	20	22	24	2	4
90.0	369.2 -10.5762	368.3 -10.5762	368.0 -10.5762	368.3 -10.5762	369.2 -10.5762	370.6 -10.5762	372.5 -10.5762	374.7 -10.5762	377.0 -10.5762	374.7 -10.5762	372.5 -10.5762	370.6 -10.5762
67.5	372.9 -10.5596	370.4 -10.5688	368.0 -10.5792	366.2 -10.5883	365.6 -10.5934	366.4 -10.5926	368.9 -10.5851	372.6 -10.5721	377.0 -10.5561	376.8 -10.5525	376.1 -10.5512	374.8 -10.5534
45.0	375.9 -10.5459	372.2 -10.5607	368.0 -10.5792	364.4 -10.5969	362.5 -10.6086	362.9 -10.6103	365.8 -10.6003	370.8 -10.5806	377.0 -10.5561	378.6 -10.5445	379.2 -10.5376	378.4 -10.5378
22.5	378.0 -10.5371	373.4 -10.5554	368.0 -10.5792	363.2 -10.6027	360.4 -10.6191	360.5 -10.6225	363.7 -10.6107	369.6 -10.5864	377.0 -10.5561	379.8 -10.5392	381.3 -10.5287	380.8 -10.5277
0.0	378.7 -10.5340	373.8 -10.5536	368.0 -10.5792	362.8 -10.6048	359.7 -10.6228	359.6 -10.6269	363.0 -10.6145	369.2 -10.5885	377.0 -10.5561	380.2 -10.5373	382.0 -10.5256	381.6 -10.5242
-22.5	378.0 -10.5371	373.4 -10.5554	368.0 -10.5792	363.2 -10.6027	360.4 -10.6191	360.5 -10.6225	363.7 -10.6107	369.6 -10.5864	377.0 -10.5561	379.8 -10.5392	381.3 -10.5287	380.8 -10.5277
-45.0	375.9 -10.5459	372.2 -10.5607	368.0 -10.5792	364.4 -10.5969	362.5 -10.6086	362.9 -10.6103	365.8 -10.6003	370.8 -10.5806	377.0 -10.5561	378.6 -10.5445	379.2 -10.5376	378.4 -10.5378
-67.5	372.9 -10.5596	370.4 -10.5688	368.0 -10.5792	366.2 -10.5883	365.6 -10.5934	366.4 -10.5926	368.9 -10.5851	372.6 -10.5721	377.0 -10.5561	376.8 -10.5525	376.1 -10.5512	374.8 -10.5534
-90.0	369.2 -10.5762	368.3 -10.5762	368.0 -10.5762	368.3 -10.5762	369.2 -10.5762	370.6 -10.5762	372.5 -10.5762	374.7 -10.5762	377.0 -10.5762	374.7 -10.5762	372.5 -10.5762	370.6 -10.5762

and oxygen chemistry also arise, is exceedingly complex. With our limited ability to acquire data and our limited understanding of the various phenomena, it is doubtful that any theoretical approach could adequately describe this region at this time, although there have been some recent attempts at constructing one-dimensional models (Shimazaki, 1968; Colegrove, Johnson, and Hanson, 1966).

3.2.2 Higher altitude results

In Figures 3, 4, and 5 are plotted diurnal density profiles at several altitudes between 300 and 750 km. Figure 3 shows densities along the equatorial plane, and Figures 4 and 5 show densities along 45° and 67.5 latitude, respectively.

We note in Figure 3 the excellent agreement, for data along the equatorial plane, between our result and that of Jacchia (1969, private communication). The agreement at 420 km is no accident. Since satellite-drag data are probably best in or near the equatorial plane and near 420-km altitude, we selected one of Jacchia's models (all of which are based on actual satellite data) to give good agreement. The results at all other latitudes and longitudes follow.

It is interesting to note that Figures 4 and 5 show our densities falling off at higher latitudes more rapidly than those of Jacchia. This leads to the question: If we start with a density distribution at 120 km that is in good agreement with Jacchia's and if in both analyses no mass is lost, what has become of our mass near the higher latitudes? The answer lies in our method of comparison. If we had matched density profiles at 45° instead of at 0° latitude, then our result would have shown a density excess near the equator and a density diminution near the poles, thus balancing the mass distribution. In all cases, we would have had our density profiles in agreement to within ±15%. Such a comparison may make the results look better; however, there still remains a basic difference between the two models in their north-south density profiles.

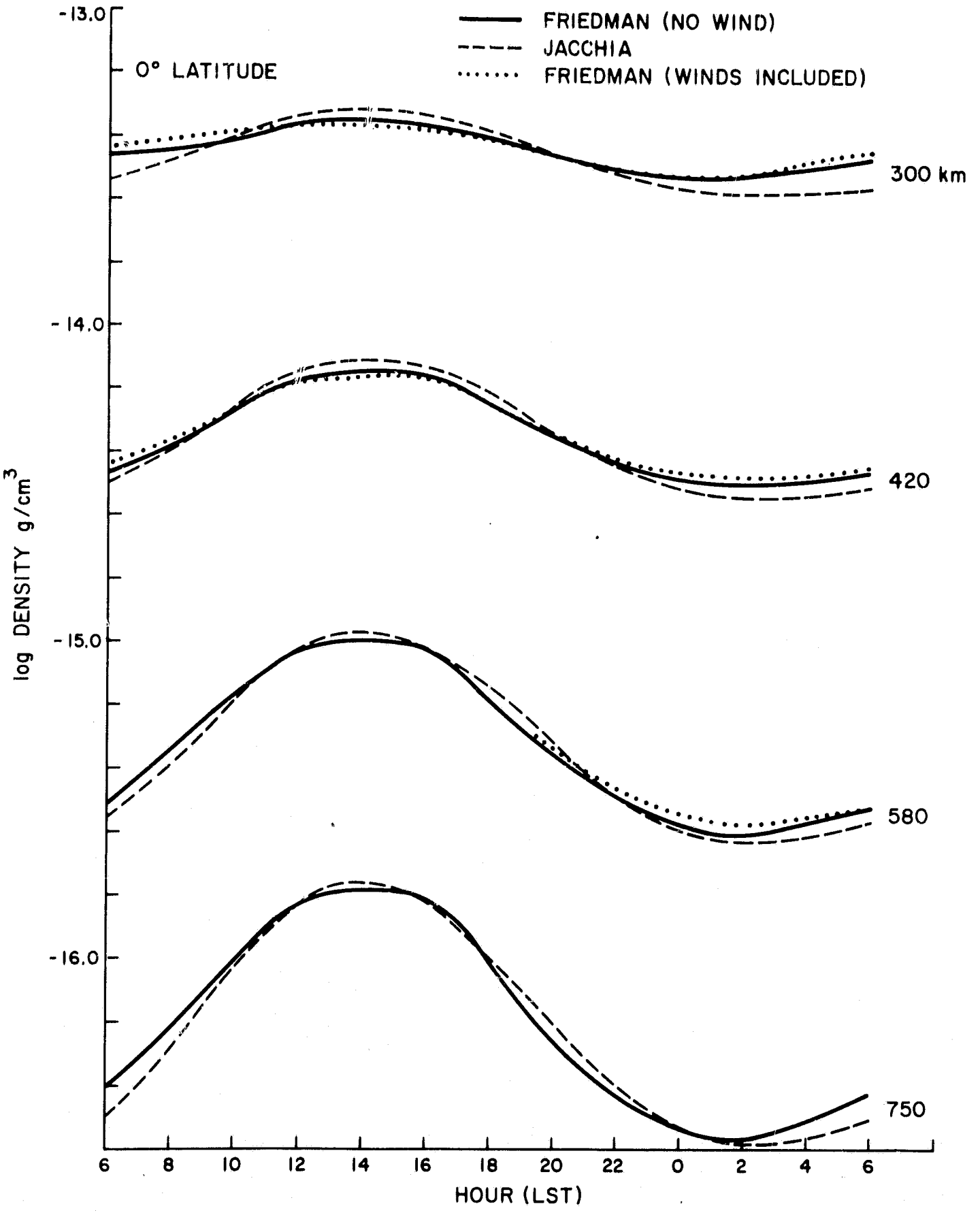

Figure 3. Diurnal density profiles in the equatorial plane for altitudes between 300 and 750 km.

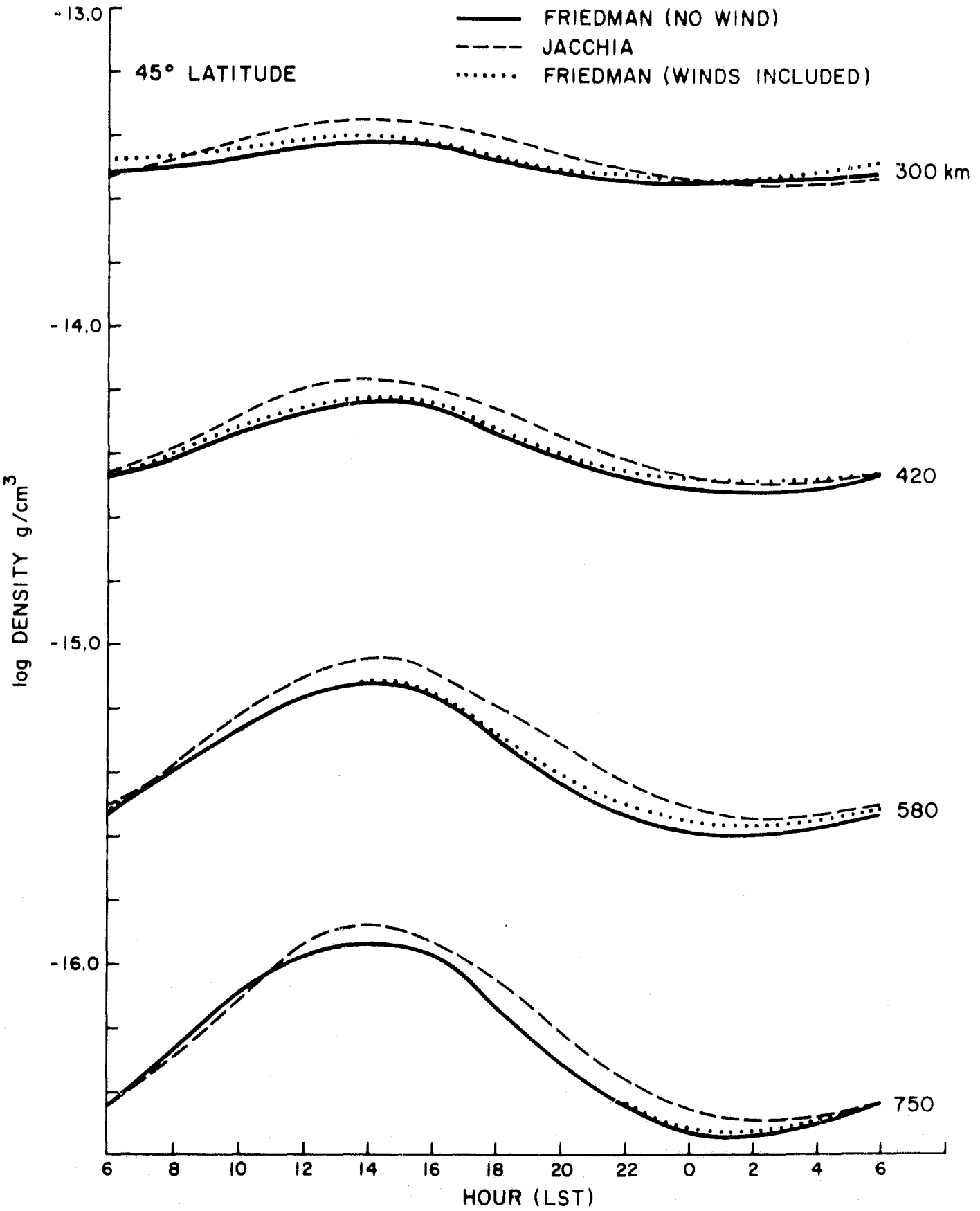

Figure 4. Diurnal density profiles at latitude 45°0 for altitudes between 300 and 750 km.

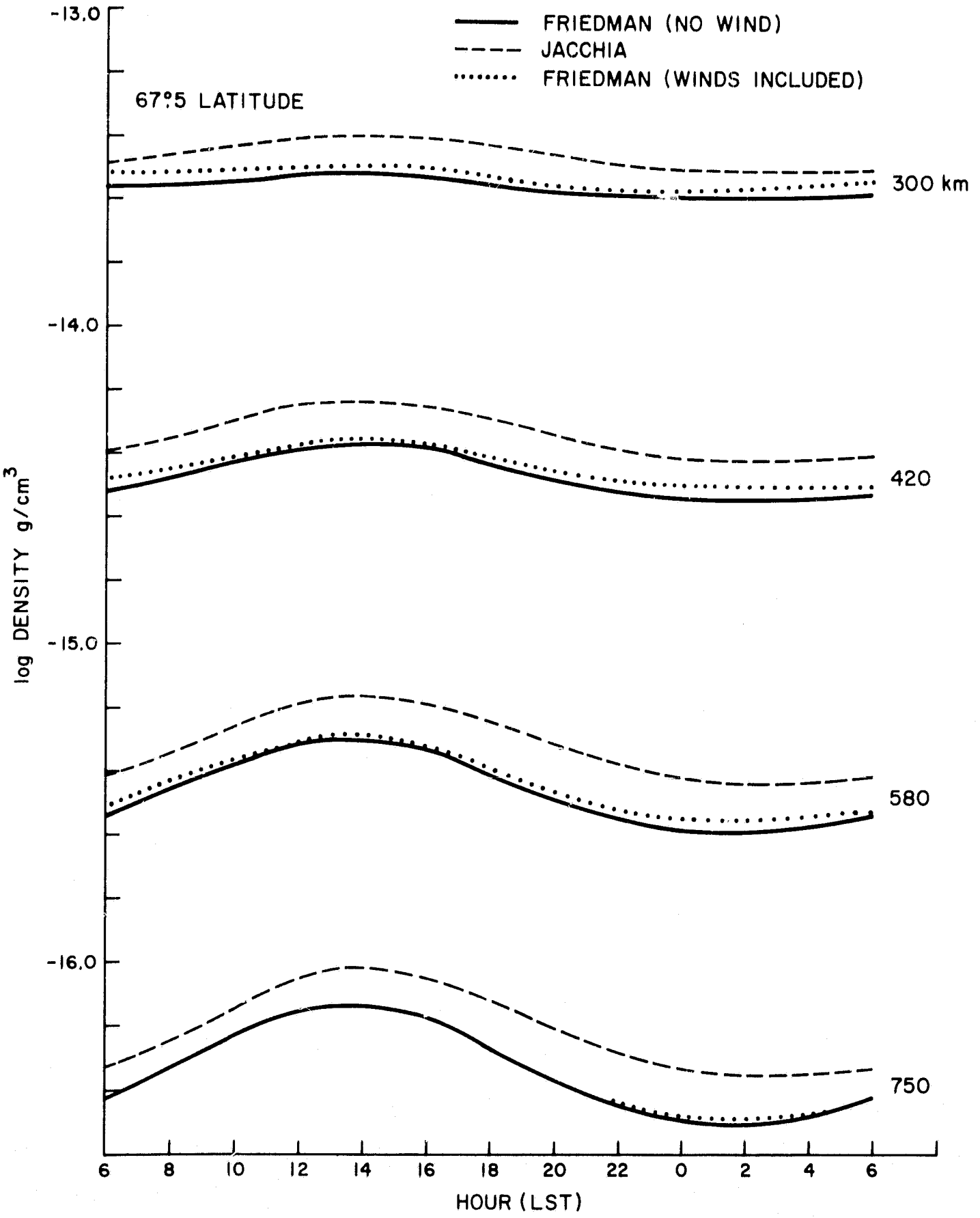

Figure 5. Diurnal density profiles at latitude 67°5 for altitudes between 300 and 750 km.

3.2.3 Temperatures

In Figures 6 and 7 we show vertical temperature profiles at 0° and 67.5 latitude at $14^h.0$ and at $2^h.0$ LST. When altitude 200 km is reached, our computed temperatures have become, and remain, higher than those used by Jacchia to generate his models. During the daytime (Figure 6) the two results agree to within 40°K, whereas at night (Figure 7) our results are some 80°K higher than Jacchia's.

Figure 8 shows diurnal temperature profiles at various altitudes between 125 and 750 km. Here again, we see that at higher altitudes our computed temperatures are consistently higher than Jacchia's.

For both sets of profiles, vertical in Figures 6 and 7 and diurnal in Figure 8, the shapes are in good agreement. Our diurnal profiles at 200 km and above show a temperature peak slightly later than Jacchia's; the times of the minima agree. It is interesting to note that our calculations consistently show that the temperature peak occurs later in the day than does the density peak between the altitudes 200 and 750 km. This is more pronounced at the lower end of the altitude range, where the densities peak near $13^h.0$ and the temperatures, near $15^h.0$. At the higher altitudes, densities peak near $14^h.0$ and the temperature peak has moved toward this hour.

It is difficult to find reasons for the differences in magnitude between our temperature profiles and Jacchia's. The major difference between the two approaches is that we are computing a three-dimensional atmosphere, while Jacchia is computing a one-dimensional vertical profile. Probably when lateral mass transfer is permitted, a higher temperature is required to support the observed densities.

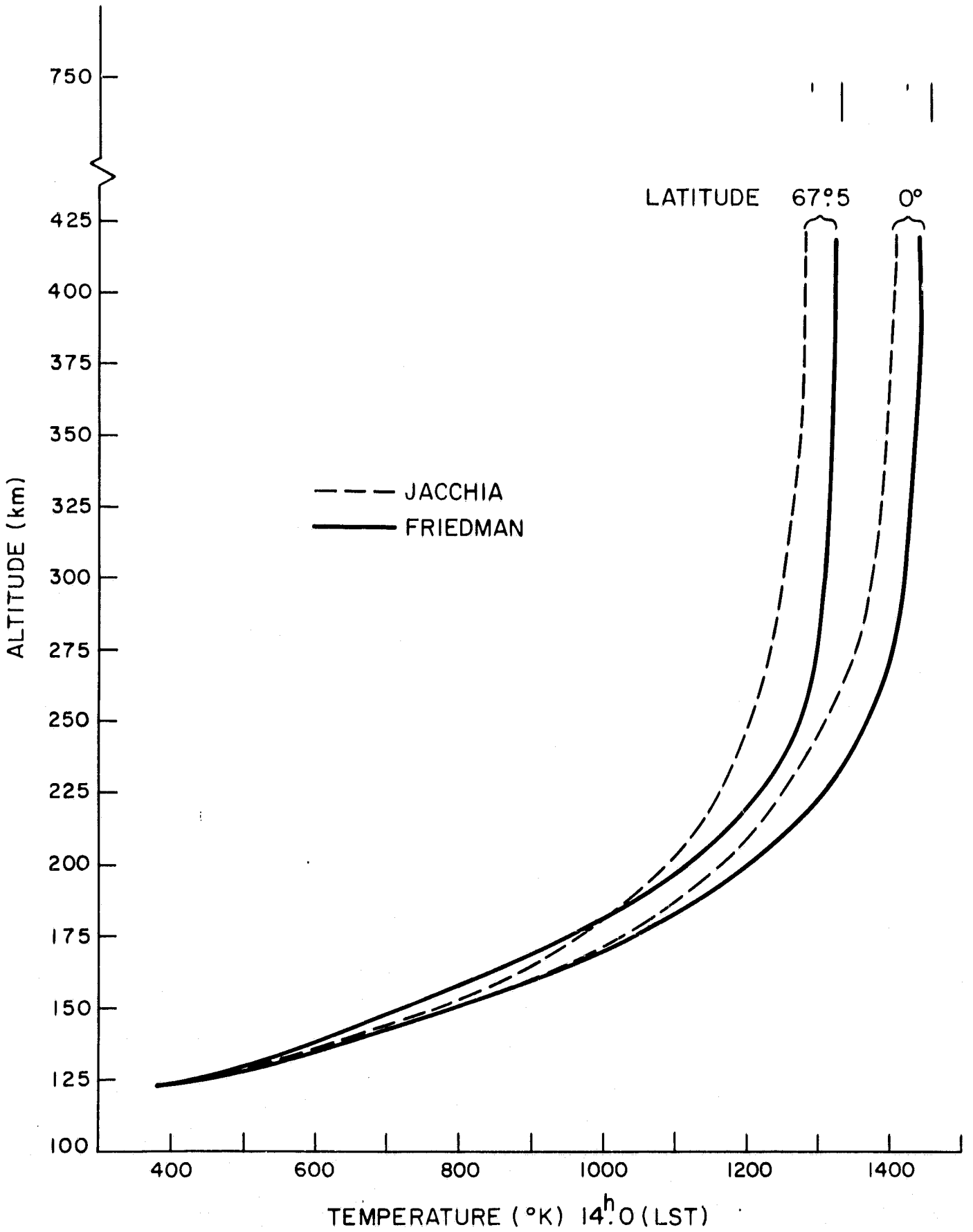

Figure 6. Vertical temperature profiles at 0° and 67°.5 latitude and at 14h.0 LST.

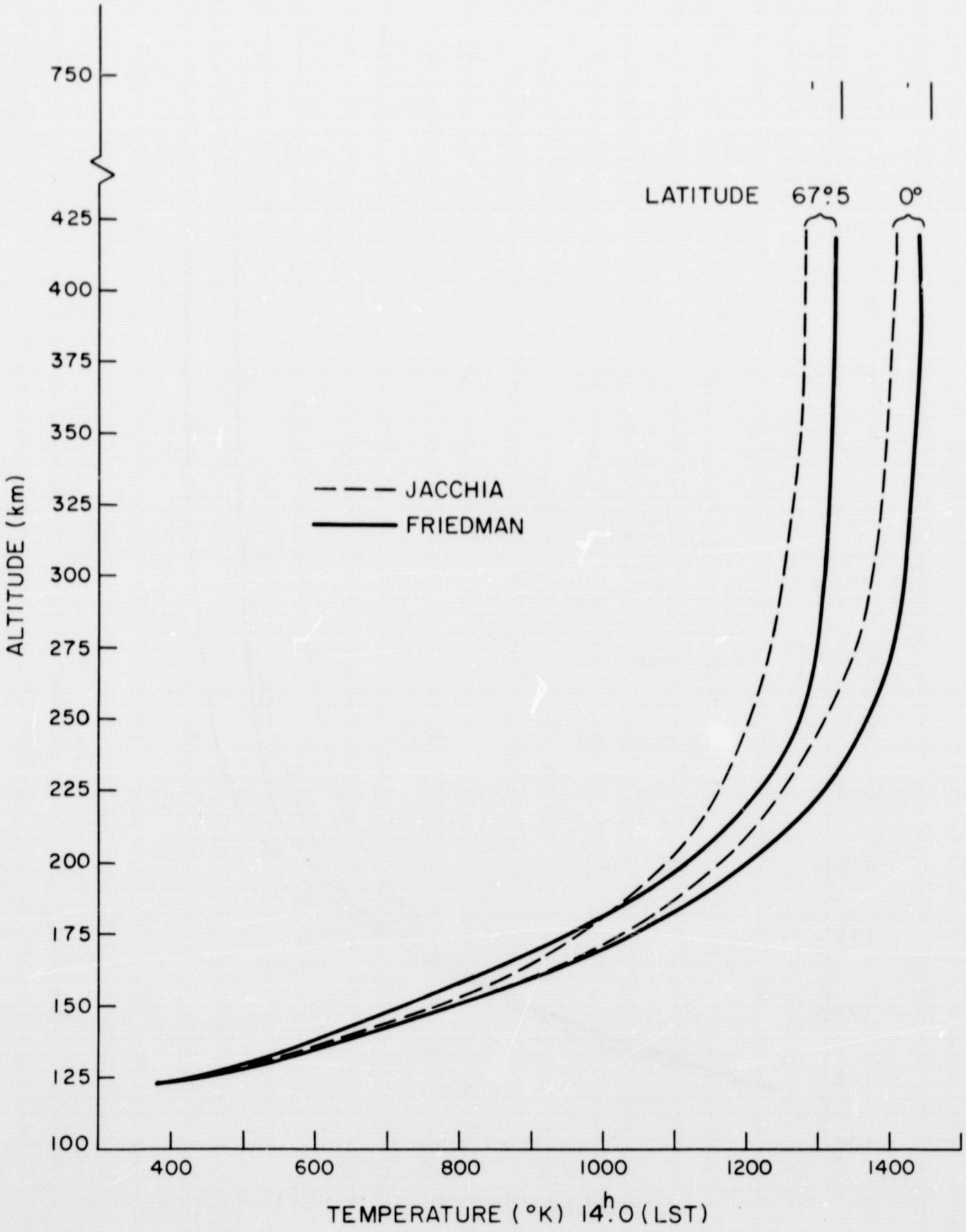

Figure 6. Vertical temperature profiles at 0° and 67°.5 latitude and at $14^{h}0$ LST.

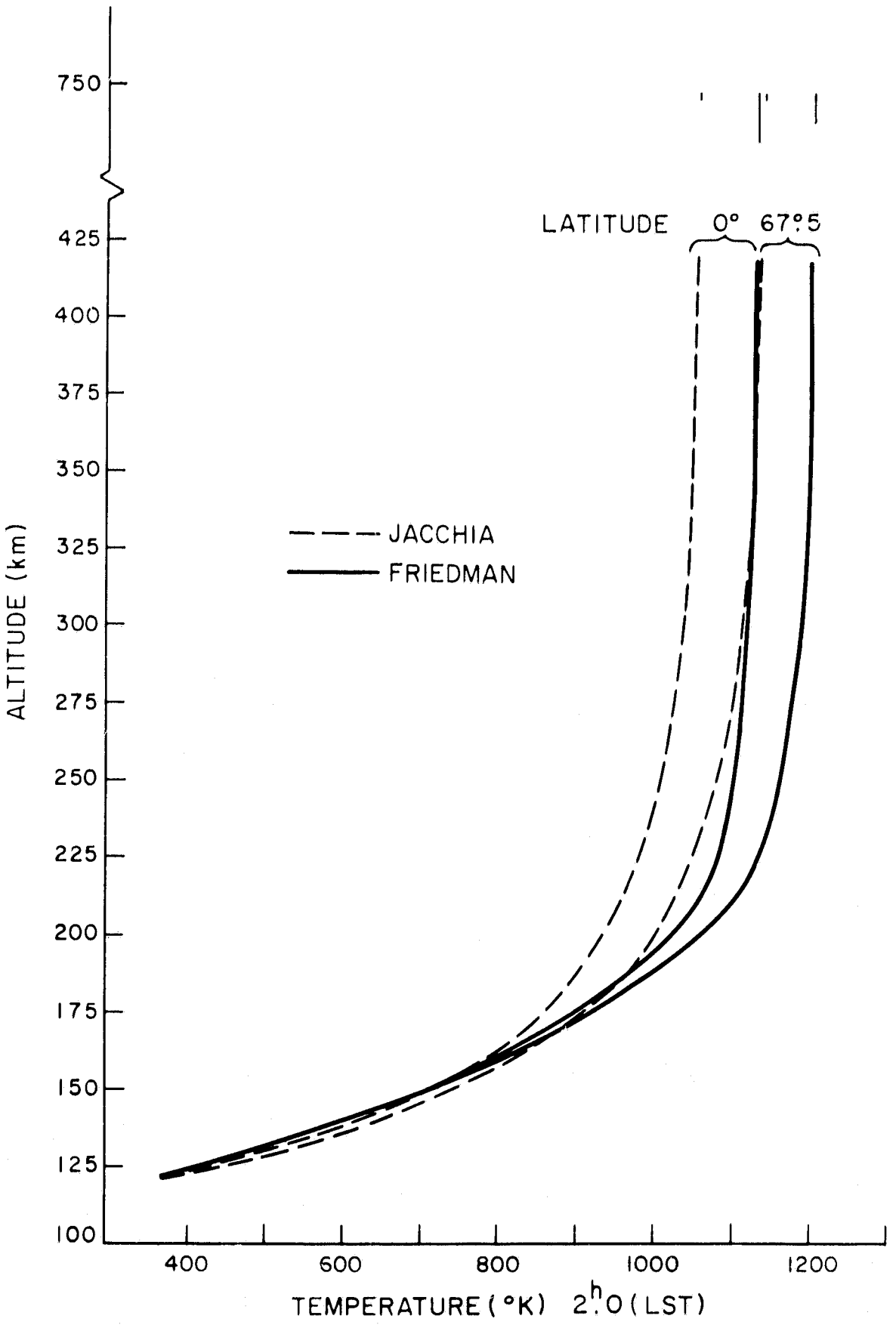

Figure 7. Vertical temperature profiles at 0° and 67°5 latitude and at $2^{h}0$ LST.

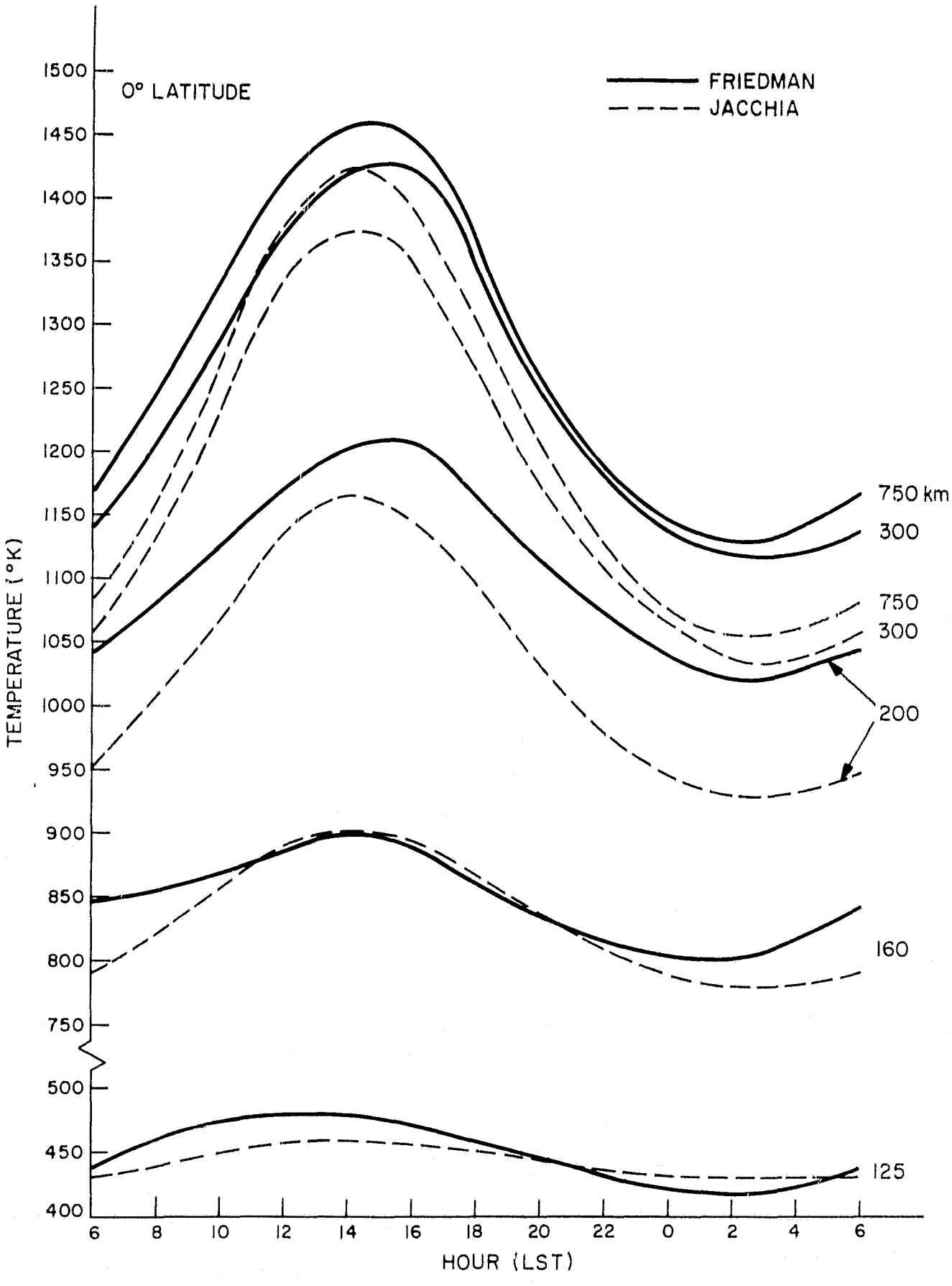

Figure 8. Diurnal temperature profiles at 0° latitude for altitudes between 125 and 750 km.

4. RESULT OF INCLUDING WINDS IN THE ANALYSIS

4.1 Momentum Equation and Boundary Conditions

In progressing from the previous section and the static (no wind) analysis to the present analysis, which includes horizontal winds, the major change is the introduction of momentum equations (9) and (10). These equations as written result from a considerable reduction of the full three-dimensional momentum equations. We chose to retain both linear and nonlinear terms since it was not clear at the outset which, if any, of these terms could be discarded.

Geisler (1966, 1967), Kohl and King (1967), and Challinor (1969) compute winds using a fixed atmosphere as a background and a linearized approximation to the momentum equation. Their results show that it might be possible to have winds of magnitude as great as 200 or 300 m/sec. In view of this, we decided not to linearize equations (9) and (10); hence, all terms on the left side of these equations are included in the analysis.

It should be pointed out that none of the authors cited above includes a term corresponding to the $\sin\theta \cos\theta$ term in equation (9). This term is the component of the centrifugal force $r\omega^2 \sin\theta \cos\theta$ along a longitudinal line due to the earth's rotation. This is a real force, and if a spherical coordinate system is used, the term must be included. These authors use a "geoid" coordinate system in which the level surfaces are equipotentials; i. e., they are normal to the resultant of the gravitational and centrifugal force vectors. Hence, horizontal winds in the level surfaces are unaffected by these forces. Such surfaces are a somewhat better approximation than are spherical surfaces to level surfaces on the earth and in the atmosphere. Therefore, a geoidal system is the most natural one for atmospheric studies.

Working in a geoidal system, we solve the momentum equations and obtain the following (dimensionless) form:

$$\frac{\mu}{\rho\omega}\frac{\partial^2 v_\theta}{\partial r^2} = -v_\phi \cos\theta\left(2+\frac{v_\phi}{\sin\theta}\right) + \left(1+\frac{v_\phi}{\sin\theta}\right)\frac{\partial v_\theta}{\partial\phi} + v_\theta\frac{\partial v_\theta}{\partial\theta}$$

$$+\frac{1}{\rho r^2\omega^2}\frac{\partial p}{\partial\theta} - \frac{1}{\rho\omega}\frac{\partial\mu}{\partial r}\frac{\partial v_\theta}{\partial r}\quad, \tag{11}$$

$$\frac{\mu}{\rho\omega}\frac{\partial^2 v_\phi}{\partial r^2} = 2\cos\theta\, v_\theta + \left(1+\frac{v_\phi}{\sin\theta}\right)\frac{\partial v_\phi}{\partial\phi} + \cot\theta\, v_\theta\, v_\phi + v_\theta\frac{\partial v_\phi}{\partial\theta}$$

$$+\frac{1}{\rho r^2\omega^2\sin\theta}\frac{\partial p}{\partial\phi} - \frac{1}{\rho\omega}\frac{\partial\mu}{\partial r}\frac{\partial v_\phi}{\partial r}\quad. \tag{12}$$

We do not include in these equations the effects of drag on the neutral constituents caused by collisions with the ionic constituents. Geisler (1966, 1967) and Kohl and King (1967) include a term to account for this effect. These authors show that the ionic drag causes a small change in the computed winds. In anticipation of the discussion on our computed results, we do not think that ionic drag will alter these results to any great extent since we already find negligible winds at altitudes where ionic drag would be important.

We did, however, set boundary conditions in the same manner as the other authors: at the lowest boundary, the velocities are set equal to zero; at the highest boundary, the radial derivative of the velocity is set equal to zero. This latter condition implies zero horizontal shear, which is reasonable because of the high kinematic viscosity at the higher altitudes. One could also reason that at sufficiently high altitudes, collisions between ions and neutrals dominate the process and therefore the neutral atmosphere would be constrained to corotate with the magnetic lines and hence with the earth. For this case, there would be no wind at higher altitudes, and an

upper boundary condition of zero wind would be appropriate. We tried some computations with this boundary condition and found negligible differences between these results and the results of zero horizontal shear conditions.

4.2 Wind Computations

In this section, the results of computing an atmosphere with winds are presented. We carried out two experiments. The first was to compute the winds with the atmosphere held fixed. This scheme for treating the problem is analogous to that used by Kohl and King (1967) and by Geisler (1966, 1967). For the second experiment, we started with the same initial atmosphere used to compute one of the models of the previous section; this time, however, we simultaneously determined temperature, density, and winds.

Figures 9a, b, and c show wind profiles computed by means of equations (11) and (12) and the fixed atmospheric model. The model used is that obtained with diurnally varying data as a lower boundary condition, discussed earlier. Figures 10a and b show the resulting winds obtained by computations that start with the same initial atmosphere as that used to compute the above model. These latter computations, as mentioned earlier, include the evolution of temperatures and densities, as well as winds, to a final equilibrium state. Figures 11 and 12 show diurnal density profiles at low altitudes for the two cases – with wind and without wind (discussed in Section 3). Curves showing density profiles at higher altitudes are given in Figures 3, 4, and 5.

4.2.1 Discussion on wind profiles

Since we are considering only the equinoctial case, we have drawn in Figures 9 and 10 only the northern hemisphere results. Our calculations show winds of greatest magnitude, about 100 m/sec, occurring near 140 km; the wind magnitude then decreases with altitude until, above 400 km, it is less than 1 m/sec. This result is contrary to those of Kohl and King (1967) and Geisler (1966, 1967), who find winds that increase with altitude, attaining magnitudes of 200 to 300 m/sec above 400 km.

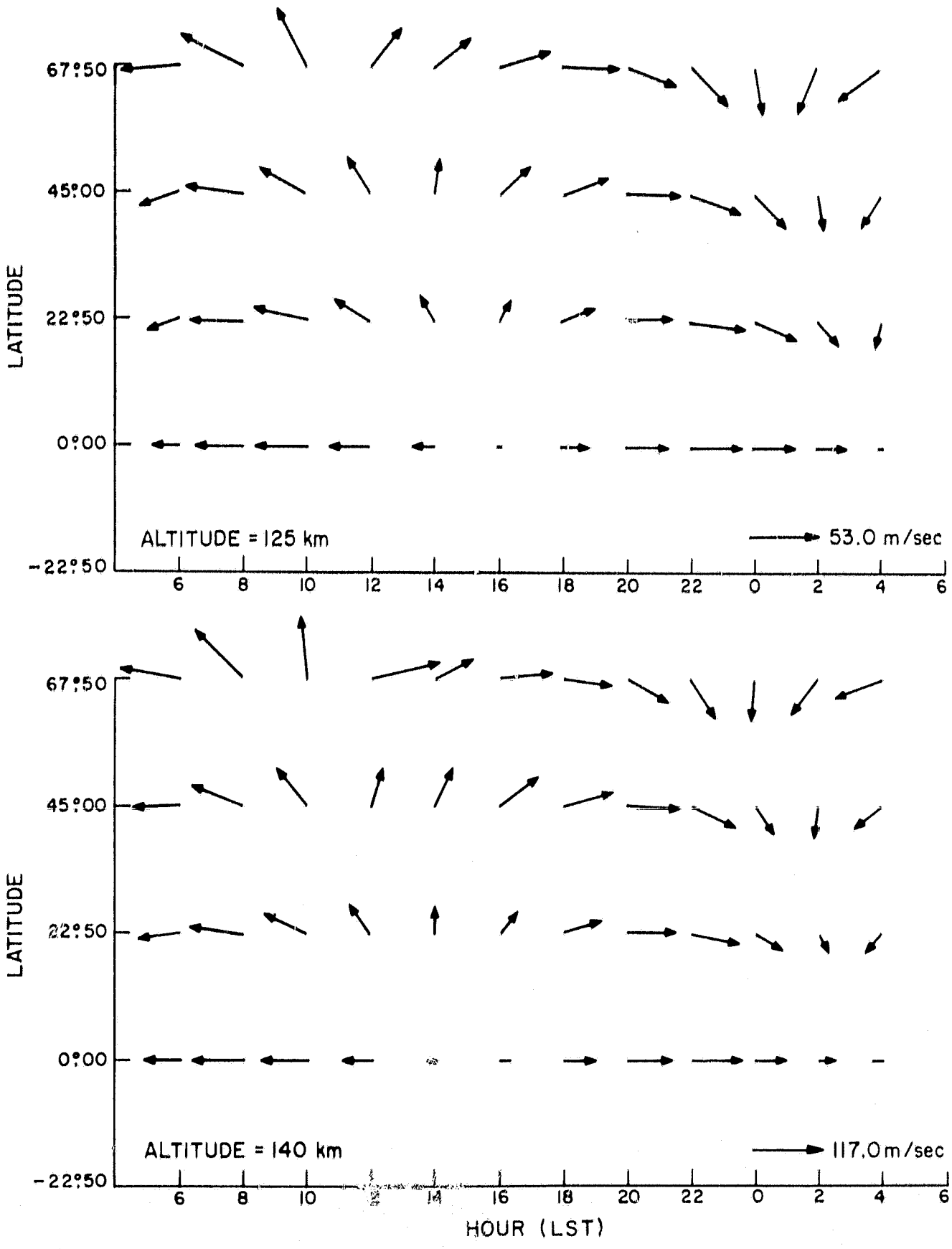

Figure 9a. Wind direction profiles for the northern hemisphere, at altitudes of 125 and 140 km. Winds are computed with a fixed atmosphere at equinoctial conditions.

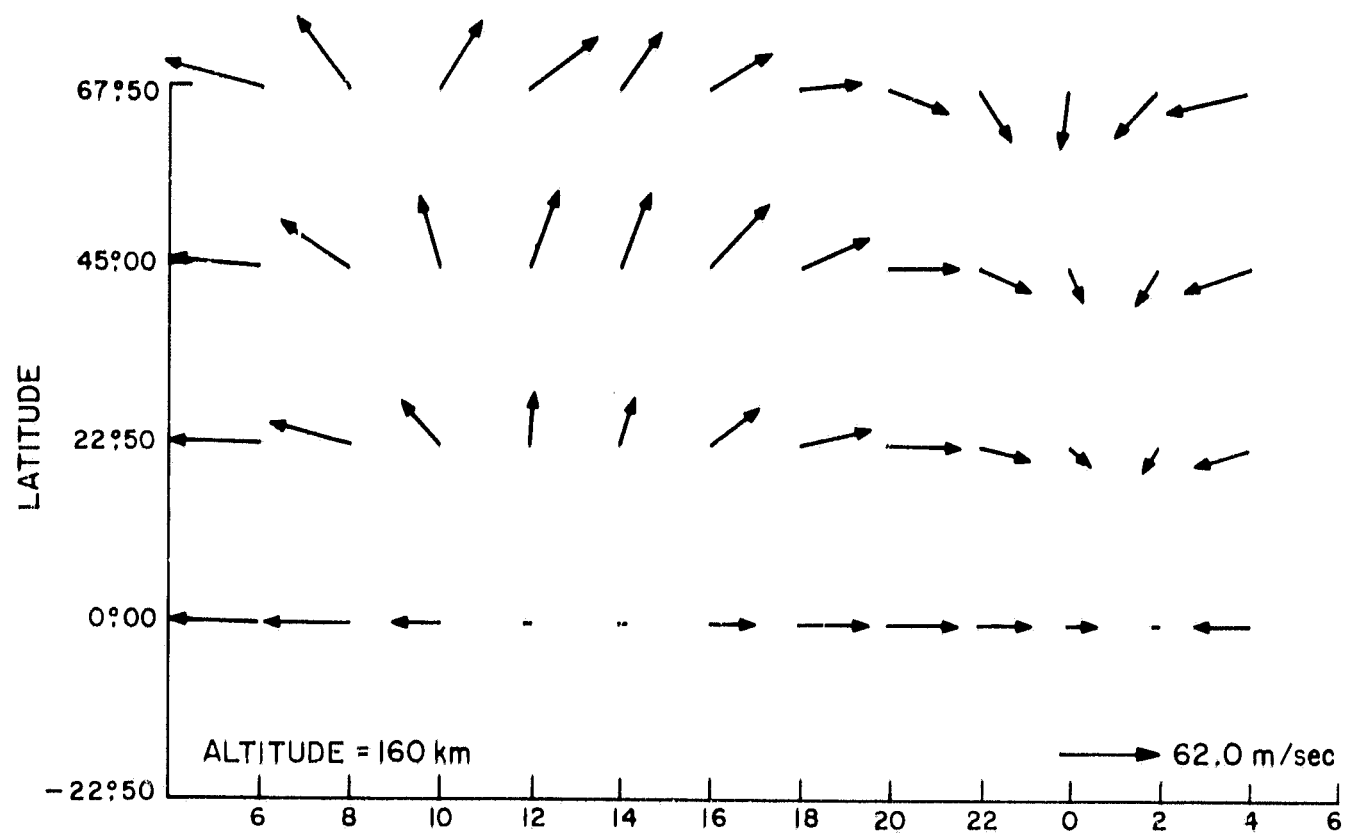

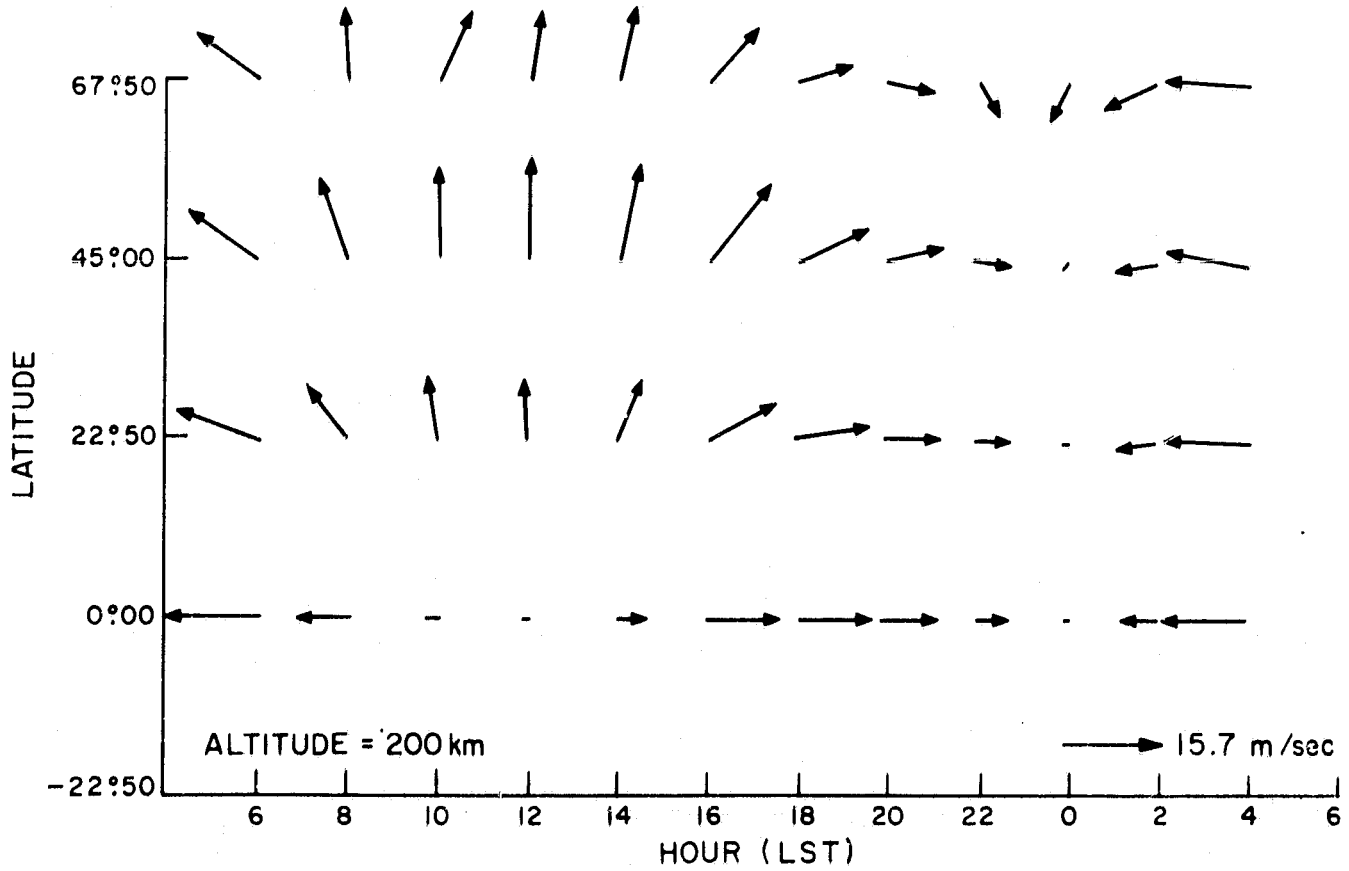

Figure 9b. Wind direction profiles for the northern hemisphere, at altitudes of 160 and 200 km. Winds are computed with a fixed atmosphere at equinoctial conditions.

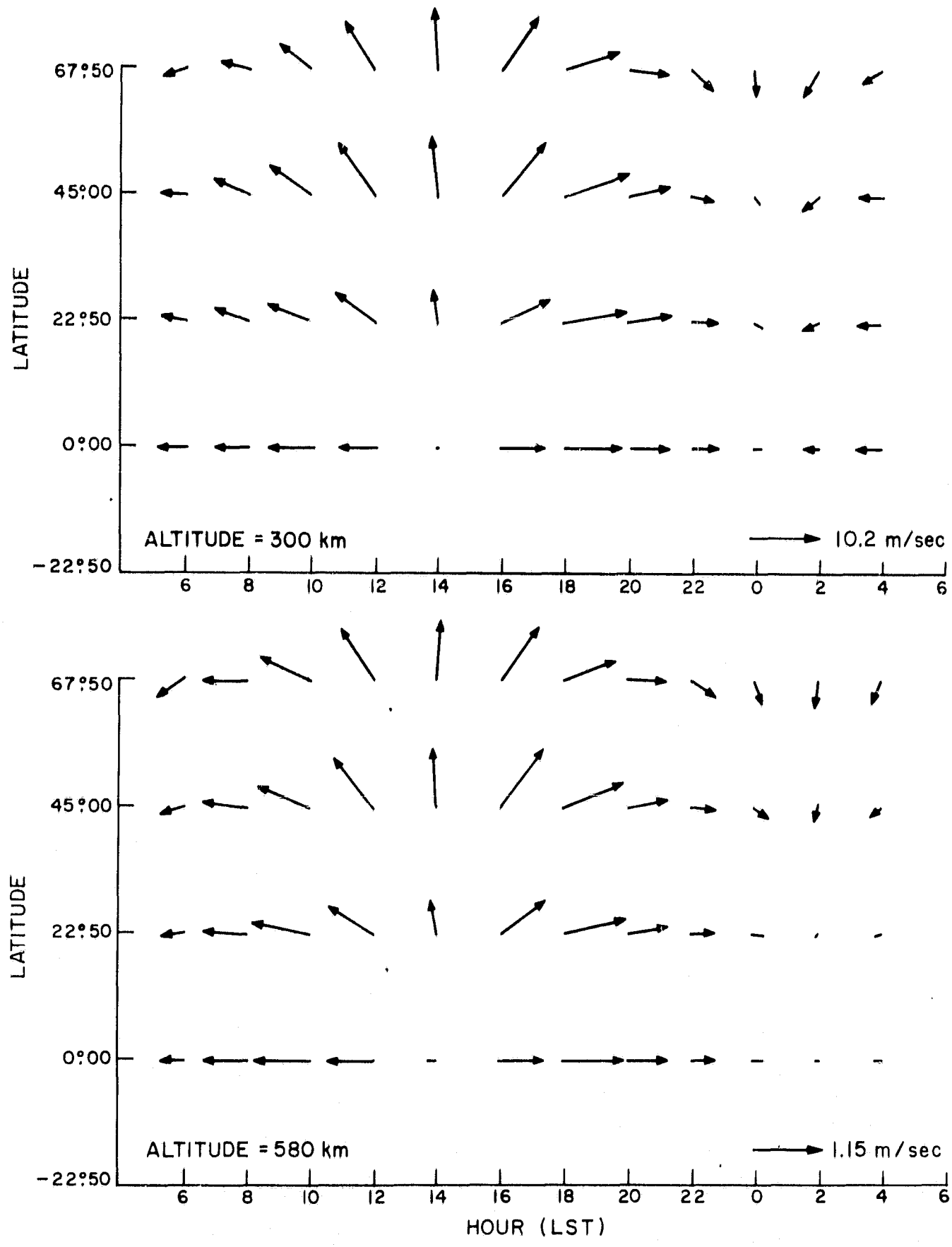

Figure 9c. Wind direction profiles for the northern hemisphere, at altitudes of 300 and 580 km. Winds are computed with a fixed atmosphere at equinoctial conditions.

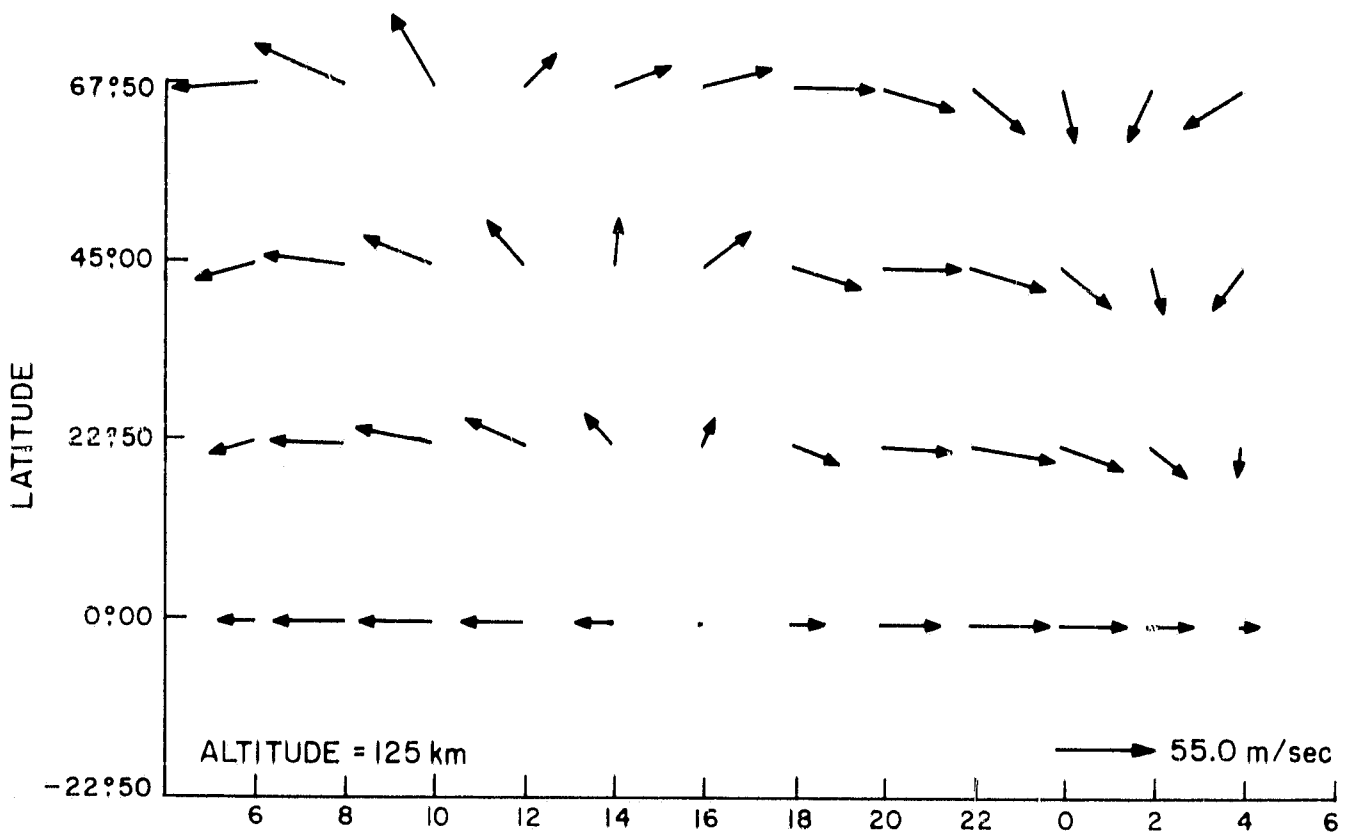

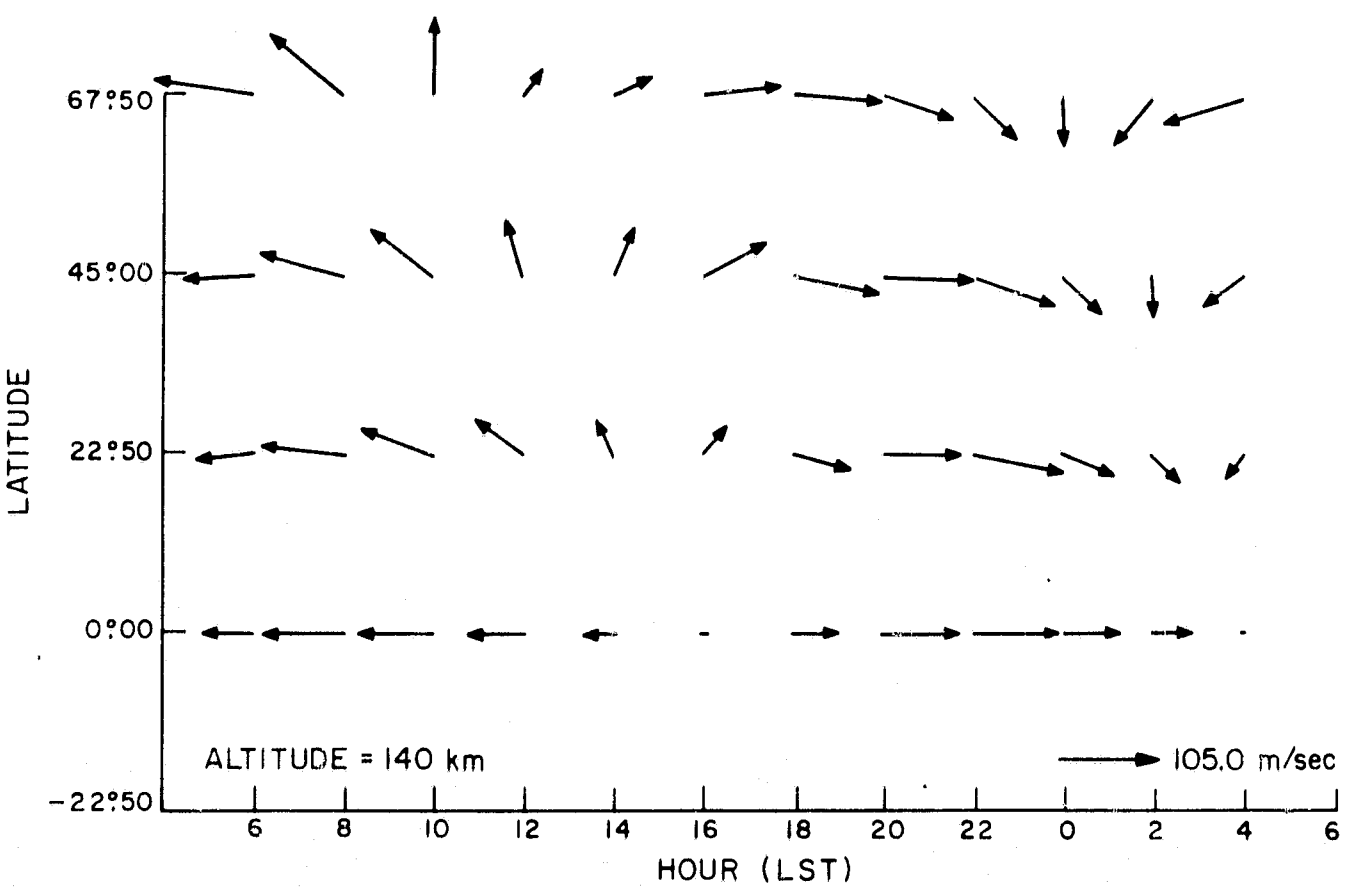

Figure 10a. Wind direction profiles for the northern hemisphere, at altitudes of 125 and 140 km. Winds are computed along with temperatures and densities at equinoctial conditions.

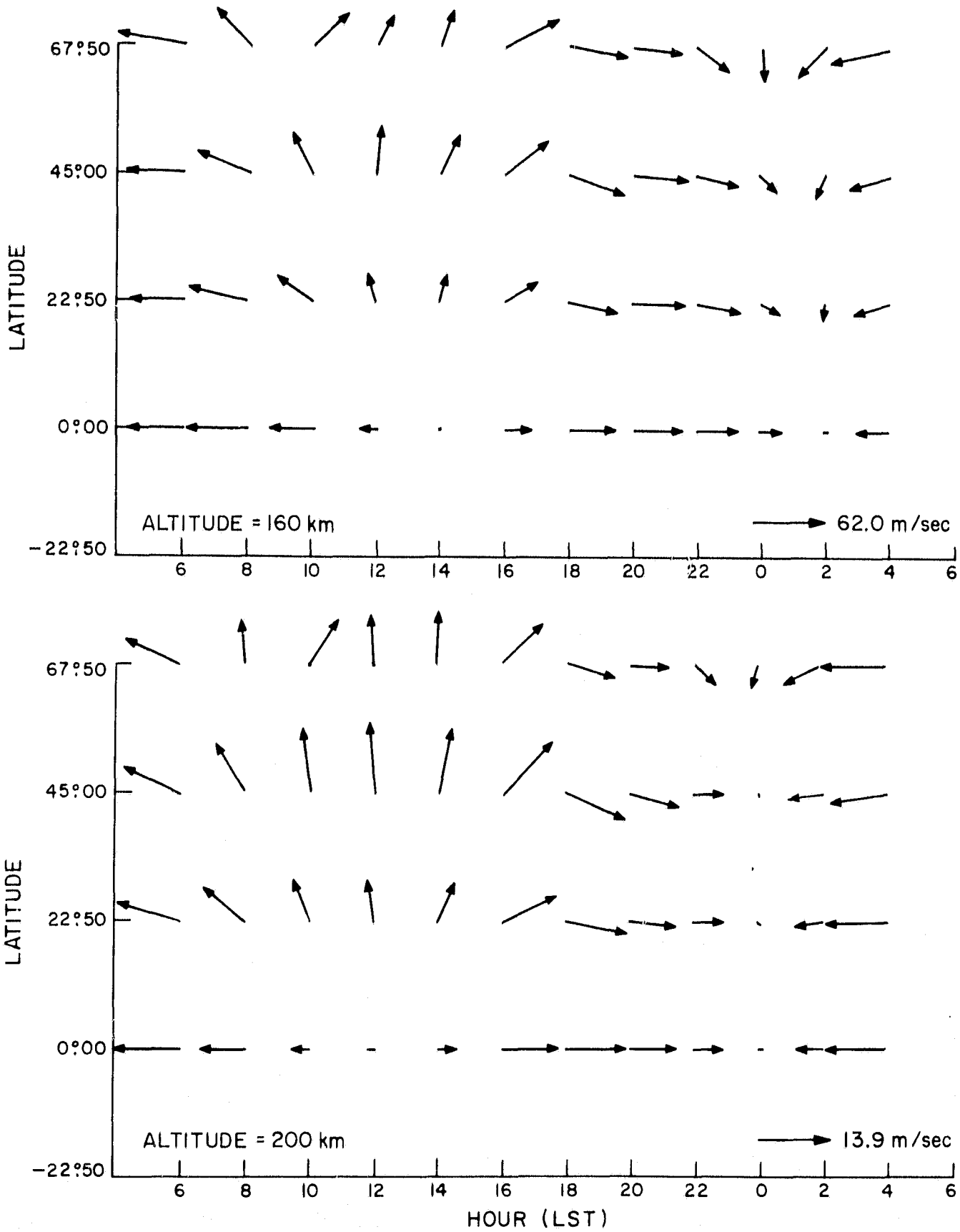

Figure 10b. Wind direction profiles for the northern hemisphere, at altitudes of 160 and 200 km. Winds are computed along with temperatures and densities at equinoctial conditions.

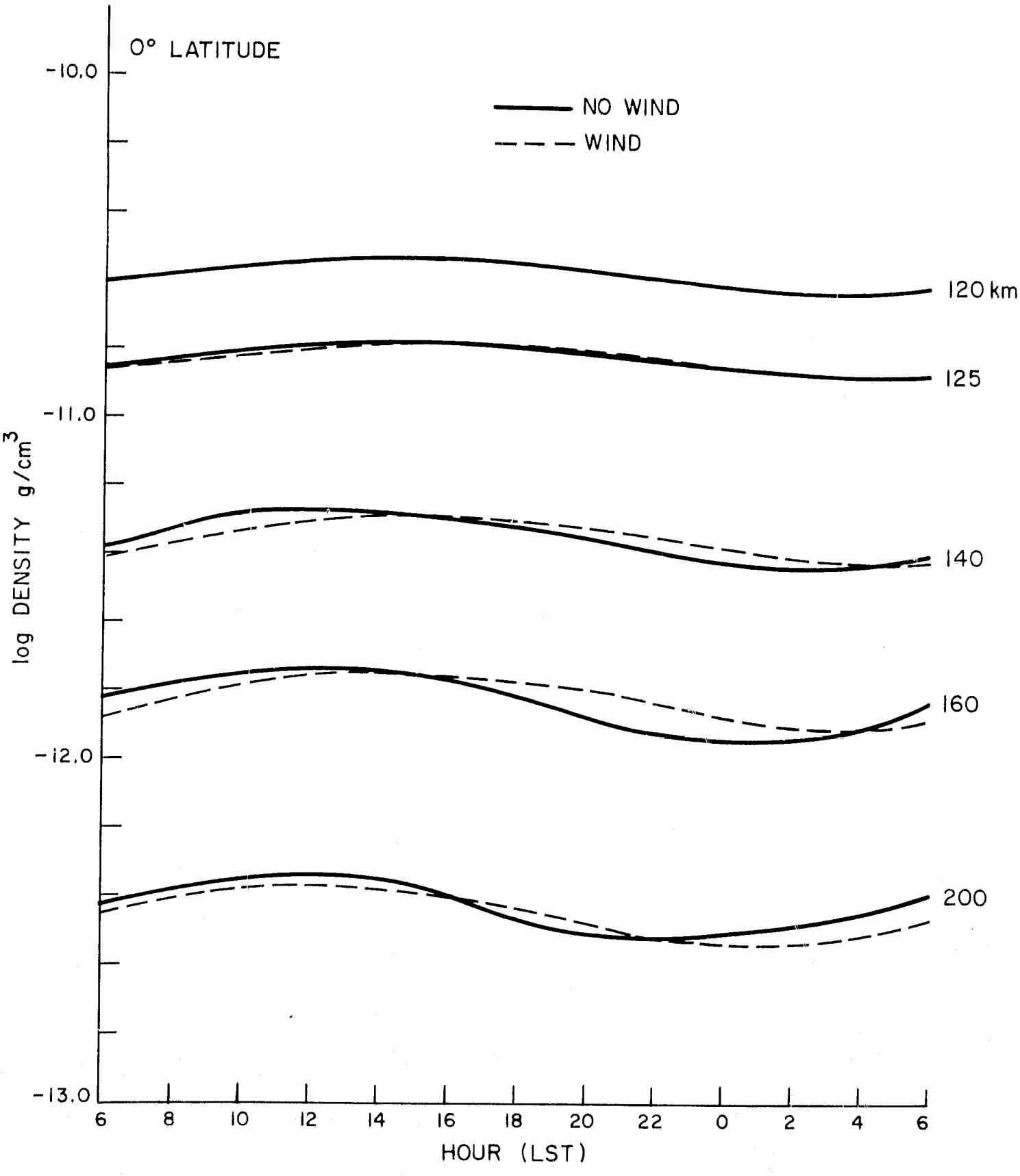

Figure 11. Comparison of diurnal density profiles in the equatorial plane for altitudes between 120 and 200 km.

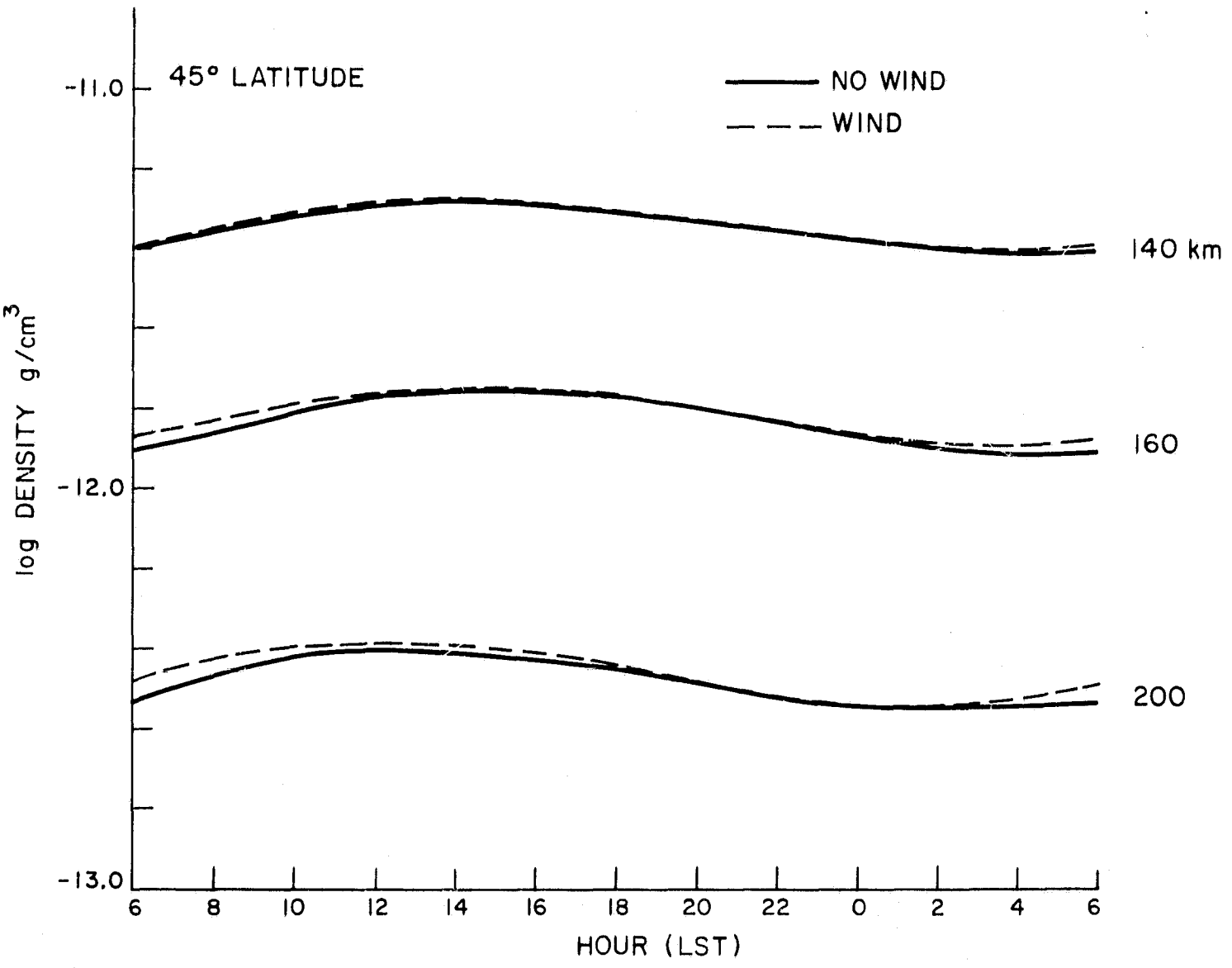

Figure 12. Comparison of diurnal density profiles at 45.0 latitude for altitudes of 140, 160, and 200 km.

We tabulate in Tables 4 to 9 computed values of the terms in the momentum equations (11) and (12). In Table 4 we define the terms of the differential equations represented by column headings 1 to 13 in Tables 5 to 9. For each altitude we have printed out data at 45° north latitude and at various times during the day, each table (5 to 8) corresponding to a different time. Table 9 presents results at the equator and $14.^{h}0$. This sampling of data is representative of results throughout the atmosphere.

From these tables, we can conclude that above 200 km the only relevant terms are the shear force and the pressure-gradient force. These are in columns 1 and 5 for the meridional velocity equation and in columns 7 and 12 for the zonal velocity equation. This implies that all other terms, including the nonlinear ones, are irrelevant in the altitude range above 200 km and that, essentially, the pressure and viscous forces are in balance.

In the altitude range above 200 km the momentum equations (11) and (12) can therefore be written as

$$\frac{\mu}{\rho\omega}\,\frac{\partial^2 v_\theta}{\partial r^2} = \frac{1}{\rho r^2 \omega^2}\,\frac{\partial p}{\partial \theta}\quad,$$

$$\frac{\mu}{\rho\omega}\,\frac{\partial^2 v_\phi}{\partial r^2} = \frac{1}{\rho r^2 \omega^2 \sin\theta}\,\frac{\partial p}{\partial \phi}\quad. \tag{13}$$

Columns 5 and 12 of Tables 5 to 9 show that the pressure gradient terms on the right side of equations (13) either remain approximately constant or increase, at most, linearly with altitude, despite the fact that density decreases exponentially. On the left side of equations (13), the controlling factor is the kinematic viscosity μ/ρ, and since μ is nearly constant above 200 km, the velocity derivative term must decrease approximately exponentially with the density. This in turn implies that the velocity itself must similarly decrease.

Table 4. Definition of column headings used in Tables 5 to 9. The numbers in the left column refer to column headings in the tables. The terms in the right column correspond to terms in the momentum equations (11) and (12); the velocities in these terms are made dimensionless by dividing the dimensioned velocities by $r\omega$ (equation (2)).

Column	Corresponding term in momentum equation
1	$\frac{\mu}{\rho\omega} \frac{\partial^2 v_\theta}{\partial r^2}$
2	$- v_\phi \cos\theta \left(2 + \frac{v_\phi}{\sin\theta}\right)$
3	$\left(1 + \frac{v_\phi}{\sin\theta}\right) \frac{\partial v_\theta}{\partial\phi}$
4	$v_\theta \frac{\partial v_\theta}{\partial\theta}$
5	$\frac{1}{\rho} \frac{\partial p}{\partial\theta} \frac{1}{r^2\omega^2}$
6	$\frac{1}{\rho\omega} \frac{\partial\mu}{\partial r} \frac{\partial v_\theta}{\partial r}$
7	$\frac{\mu}{\rho\omega} \frac{\partial^2 v_\phi}{\partial r^2}$
8	$2 \cos\theta\, v_\theta$
9	$\left(1 + \frac{v_\phi}{\sin\theta}\right) \frac{\partial v_\phi}{\partial\phi}$
10	$\cot\theta\, v_\theta\, v_\phi$
11	$v_\theta \frac{\partial v_\phi}{\partial\theta}$
12	$\frac{1}{\rho} \frac{\partial p}{\partial\theta} \frac{1}{r^2\omega^2 \sin\theta}$
13	$\frac{1}{\rho\omega} \frac{\partial\mu}{\partial r} \frac{\partial v_\phi}{\partial r}$

Table 5. Numerical values at 45°0 latitude and 8.^{h}0 LST of terms in the momentum equations (11) and (12). Column headings are defined in Table 4.

ALTITUDE, KM (1)	(2)	(3)	(4)	(5)	(6)	(7)	(8)	(9)	(10)	(11)	(12)	(13)
125.0												
3.05E-02	1.22E-01	-5.31E-02	-1.04E-03	-3.97E-02	-1.85E-03	6.74E-02	-2.18E-02	-4.00E-02	1.42E-03	-4.85E-04	1.22E-01	-6.05E-03
140.0												
5.34E-02	2.14E-01	-9.96E-02	-8.28E-03	-5.29E-02	6.77E-05	1.27E-01	-8.88E-02	-3.07E-02	1.08E-02	1.30E-03	2.36E-01	1.74E-03
160.0												
6.01E-02	1.19E-01	-7.20E-02	-5.22E-03	2.00E-02	2.06E-03	2.40E-01	-6.84E-02	2.77E-02	4.36E-03	2.80E-03	2.86E-01	1.25E-02
180.0												
1.35E-01	4.43E-02	-3.69E-02	-3.41E-04	1.31E-01	3.34E-03	3.25E-01	-5.20E-02	4.07E-02	1.18E-03	1.51E-03	3.44E-01	9.82E-03
200.0												
2.56E-01	1.61E-02	-1.54E-02	1.61E-04	2.61E-01	5.23E-03	3.67E-01	-3.49E-02	2.49E-02	2.84E-04	4.49E-04	3.82E-01	6.13E-03
220.0												
4.12E-01	6.87E-03	-5.79E-03	1.15E-04	4.17E-01	7.13E-03	3.41E-01	-2.15E-02	1.09E-02	7.41E-05	1.05E-04	3.55E-01	3.83E-03
240.0												
5.23E-01	4.31E-03	-2.66E-03	4.81E-05	5.29E-01	7.53E-03	3.11E-01	-1.24E-02	2.97E-03	2.68E-05	2.36E-05	3.22E-01	1.94E-03
260.0												
5.82E-01	6.22E-03	-3.22E-03	4.94E-05	5.75E-01	-4.14E-03	3.24E-01	-1.18E-02	-1.30E-03	3.69E-05	1.69E-05	3.32E-01	-5.31E-03
300.0												
5.62E-01	8.57E-03	-4.26E-03	3.65E-05	5.72E-01	1.47E-02	4.74E-01	-9.81E-03	-5.15E-03	4.22E-05	1.09E-05	4.95E-01	5.61E-03
340.0												
5.34E-01	5.77E-03	-2.85E-03	6.95E-06	5.46E-01	1.55E-02	6.97E-01	-4.22E-03	-4.16E-03	1.22E-05	2.13E-06	7.17E-01	1.20E-02
380.0												
5.11E-01	3.60E-03	-1.80E-03	1.34E-06	5.20E-01	1.07E-02	9.62E-01	-1.85E-03	-2.64E-03	3.33E-06	4.59E-07	9.79E-01	1.34E-02
420.0												
5.06E-01	2.25E-03	-1.13E-03	3.28E-07	5.11E-01	6.34E-03	1.25E+00	-9.19E-04	-1.60E-03	1.04E-06	1.15E-07	1.27E+00	1.14E-02
460.0												
5.28E-01	1.95E-03	-9.82E-04	1.85E-07	5.28E-01	5.77E-04	1.57E+00	-6.91E-04	-1.32E-03	6.76E-07	5.93E-08	1.57E+00	-3.63E-04
520.0												
5.66E-01	1.59E-03	-8.00E-04	1.03E-07	5.67E-01	1.45E-03	1.95E+00	-5.18E-04	-1.02E-03	4.13E-07	3.04E-08	1.95E+00	4.18E-03
580.0												
6.37E-01	1.10E-03	-5.57E-04	4.52E-08	6.35E-01	-1.56E-03	2.32E+00	-3.45E-04	-6.54E-04	1.89E-07	1.45E-08	2.32E+00	-4.63E-03
660.0												
7.36E-01	7.24E-04	-3.71E-04	1.84E-08	7.23E-01	-1.26E-02	2.76E+00	-2.21E-04	-3.99E-04	8.02E-08	7.18E-09	2.72E+00	-4.12E-02
750.0												
8.72E-01	4.06E-04	-2.08E-04	5.33E-09	8.16E-01	-5.62E-02	3.29E+00	-1.20E-04	-2.14E-04	2.44E-08	2.37E-09	3.10E+00	-1.38E-01

Table 6. Numerical values at 45.°0 latitude and 14.^{h}0 LST of terms in the momentum equations (11) and (12). Column headings are defined in Table 4.

ALTITUDE, KM (1)	(2)	(3)	(4)	(5)	(6)	(7)	(8)	(9)	(10)	(11)	(12)	(13)
125.0												
6.11E-02	-7.57E-03	8.25E-03	2.00E-03	5.50E-02	-3.47E-03	2.34E-02	-8.18E-02	8.59E-02	-3.09E-04	6.27E-03	1.47E-02	1.40E-03
140.0												
7.03E-02	-7.41E-02	5.24E-02	1.22E-02	8.04E-02	6.66E-04	2.92E-02	-1.71E-01	1.76E-01	-6.11E-03	1.57E-02	1.66E-02	1.76E-03
160.0												
6.67E-02	-4.63E-02	3.43E-02	2.00E-03	8.18E-02	5.14E-03	-3.86E-02	-1.25E-01	5.10E-02	-2.84E-03	7.95E-04	3.40E-02	-3.88E-03
180.0												
2.99E-01	-1.68E-02	2.06E-02	8.44E-04	3.03E-01	8.20E-03	-2.87E-02	-7.45E-02	1.91E-02	-6.19E-04	-5.90E-04	2.49E-02	-2.97E-03
200.0												
5.35E-01	-7.03E-03	1.08E-02	3.48E-04	5.40E-01	8.97E-03	-2.14E-02	-4.33E-02	2.61E-02	-1.52E-04	-1.98E-04	-5.69E-03	-1.91E-03
220.0												
7.11E-01	-2.91E-03	5.27E-03	1.33E-04	7.18E-01	9.27E-03	-5.03E-02	-2.60E-02	1.54E-02	-3.78E-05	-5.13E-05	-4.14E-02	-1.78E-03
240.0												
8.31E-01	-6.83E-04	2.41E-03	5.08E-05	8.37E-01	7.86E-03	-5.01E-02	-1.65E-02	1.01E-02	-5.62E-06	-1.32E-05	-4.53E-02	-1.57E-03
260.0												
9.34E-01	6.35E-04	1.46E-03	6.03E-05	9.22E-01	-1.03E-02	-1.68E-02	-1.91E-02	1.29E-02	6.06E-06	-5.96E-06	-1.21E-02	-1.54E-03
300.0												
1.06E+00	1.90E-03	2.85E-04	5.87E-05	1.08E+00	1.76E-02	6.19E-02	-2.06E-02	1.10E-02	1.96E-05	6.08E-06	7.14E-02	-2.19E-05
340.0												
1.22E+00	1.43E-03	-3.12E-04	1.53E-05	1.24E+00	2.38E-02	1.34E-01	-1.15E-02	6.76E-03	8.21E-06	5.03E-06	1.41E-01	2.24E-03
380.0												
1.39E+00	8.05E-04	-3.27E-04	4.03E-06	1.41E+00	2.14E-02	1.79E-01	-6.38E-03	4.04E-03	2.57E-06	2.33E-06	1.85E-01	2.95E-03
420.0												
1.57E+00	4.03E-04	-2.16E-04	1.24E-06	1.59E+00	1.67E-02	1.96E-01	-3.72E-03	2.51E-03	7.50E-07	9.90E-07	2.00E-01	2.53E-03
460.0												
1.77E+00	2.50E-04	-1.73E-04	8.37E-07	1.77E+00	9.11E-05	1.87E-01	-3.10E-03	2.17E-03	3.87E-07	7.79E-07	1.89E-01	7.07E-04
520.0												
1.99E+00	1.31E-04	-1.09E-04	5.31E-07	2.00E+00	1.11E-02	1.52E-01	-2.46E-03	1.78E-03	1.62E-07	5.06E-07	1.54E-01	1.12E-03
580.0												
2.22E+00	5.25E-05	-4.79E-05	2.54E-07	2.22E+00	1.51E-03	1.08E-01	-1.67E-03	1.22E-03	4.39E-08	2.24E-07	1.08E-01	1.43E-04
660.0												
2.48E+00	1.72E-05	-1.69E-05	1.07E-07	2.47E+00	-1.38E-02	6.39E-02	-1.09E-03	8.02E-04	9.34E-09	8.95E-08	6.36E-02	-5.60E-04
750.0												
2.80E+00	2.50E-06	-1.20E-05	2.85E-08	2.72E+00	-8.32E-02	2.15E-02	-6.02E-04	4.44E-04	7.54E-10	2.81E-08	2.07E-02	-9.34E-04

Table 7. Numerical values at 45°.0 latitude and 20^{h}.0 LST of terms in the momentum equations (11) and (12). Column headings are defined in Table 4.

ALTITUDE, KM (1)	(2)	(3)	(4)	(5)	(6)	(7)	(8)	(9)	(10)	(11)	(12)	(13)
125.0												
-3.41E-02	-1.38E-01	6.58E-02	-9.52E-04	3.87E-02	9.67E-05	-1.02E-01	1.66E-04	-1.10E-02	1.07E-05	-6.88E-07	-8.59E-02	5.10E-03
140.0												
-7.39E-02	-3.23E-01	1.48E-01	-4.63E-03	1.03E-01	-2.22E-03	-2.22E-01	1.57E-02	-6.43E-02	2.22E-03	2.00E-04	-1.78E-01	-2.51E-03
160.0												
6.26E-02	-1.51E-01	7.51E-02	-4.64E-04	1.39E-01	-1.68E-04	-3.52E-01	-1.52E-02	-5.72E-02	-1.07E-03	-1.81E-04	-2.93E-01	-1.40E-02
180.0												
1.13E-01	-6.10E-02	3.21E-02	-5.82E-05	1.43E-01	1.25E-03	-4.38E-01	-1.18E-02	-2.99E-02	-3.49E-04	-4.70E-05	-4.09E-01	-1.29E-02
200.0												
1.39E-01	-2.75E-02	1.44E-02	1.59E-05	1.54E-01	1.16E-03	-5.22E-01	-9.71E-03	-1.59E-02	-1.32E-04	-1.37E-05	-5.07E-01	-1.02E-02
220.0												
1.76E-01	-1.37E-02	7.03E-03	2.46E-05	1.85E-01	1.63E-03	-5.55E-01	-8.24E-03	-8.98E-03	-5.60E-05	-5.09E-06	-5.46E-01	-8.05E-03
240.0												
2.52E-01	-7.98E-03	4.13E-03	1.84E-05	2.58E-01	1.81E-03	-5.50E-01	-6.73E-03	-5.46E-03	-2.67E-05	-2.49E-06	-5.43E-01	-5.33E-03
260.0												
3.58E-01	-9.30E-03	4.89E-03	3.14E-05	3.56E-01	-6.13E-03	-5.68E-01	-8.74E-03	-6.33E-03	-4.04E-05	-4.61E-06	-5.46E-01	6.68E-03
300.0												
4.61E-01	-1.06E-02	5.75E-03	3.56E-05	4.76E-01	1.00E-02	-6.69E-01	-9.29E-03	-7.02E-03	-4.89E-05	-6.76E-06	-6.64E-01	-1.07E-02
340.0												
5.58E-01	-6.24E-03	3.55E-03	1.01E-05	5.75E-01	1.43E-02	-8.20E-01	-4.92E-03	-4.03E-03	-1.53E-05	-2.40E-06	-8.27E-01	-1.57E-02
380.0												
6.46E-01	-3.58E-03	2.08E-03	2.66E-06	6.59E-01	1.22E-02	-1.02E+00	-2.50E-03	-2.24E-03	-4.46E-06	-7.20E-07	-1.03E+00	-1.50E-02
420.0												
7.27E-01	-2.12E-03	1.24E-03	7.62E-07	7.36E-01	8.75E-03	-1.24E+00	-1.32E-03	-1.29E-03	-1.39E-06	-2.17E-07	-1.25E+00	-1.19E-02
460.0												
7.99E-01	-1.75E-03	1.02E-03	4.23E-07	8.01E-01	1.29E-03	-1.49E+00	-9.67E-04	-1.04E-03	-8.49E-07	-1.25E-07	-1.49E+00	-3.09E-04
520.0												
8.41E-01	-1.38E-03	8.02E-04	2.04E-07	8.44E-01	2.59E-03	-1.79E+00	-6.63E-04	-8.17E-04	-4.59E-07	-6.72E-08	-1.79E+00	-4.37E-03
580.0												
8.65E-01	-9.39E-04	5.49E-04	6.89E-08	8.63E-01	-2.54E-03	-2.11E+00	-3.81E-04	-5.64E-04	-1.79E-07	-2.85E-08	-2.11E+00	4.02E-03
660.0												
8.64E-01	-6.20E-04	3.64E-04	2.02E-08	8.47E-01	-1.70E-02	-2.56E+00	-2.06E-04	-3.82E-04	-6.40E-08	-1.08E-08	-2.52E+00	3.79E-02
750.0												
8.50E-01	-3.53E-04	2.01E-04	4.19E-09	7.93E-01	-5.64E-02	-3.18E+00	-9.66E-05	-2.19E-04	-1.71E-08	-2.68E-09	-3.00E+00	1.84E-01

Table 8. Numerical values at 45°.0 latitude and 2.^{h}0 LST of terms in the momentum equations (11) and (12). Column headings are defined in Table 4.

ALTITUDE, KM (1)	(2)	(3)	(4)	(5)	(6)	(7)	(8)	(9)	(10)	(11)	(12)	(13)
125.0	-8.35E-02	-1.85E-02	-5.08E-03	-3.11E-03	-5.38E-02	3.08E-03	-2.52E-02	8.38E-02	-8.10E-02	7.66E-04	4.83E-03	-3.35E-02	1.40E-04
140.0	-1.19E-01	-6.29E-03	-2.48E-02	-7.79E-03	-8.44E-02	-3.88E-03	-5.83E-02	1.42E-01	-1.63E-01	4.44E-04	1.70E-02	-5.56E-02	-1.52E-03
160.0	-8.46E-02	2.02E-02	-9.38E-03	-1.49E-03	-1.02E-01	-8.01E-03	-8.50E-02	5.59E-02	-1.03E-01	-5.71E-04	2.23E-03	-4.18E-02	-2.62E-03
180.0	-1.27E-01	2.33E-02	-7.54E-03	-1.48E-04	-1.49E-01	-6.19E-03	4.85E-03	1.80E-02	-4.65E-02	-2.12E-04	2.21E-04	3.44E-02	9.92E-04
200.0	-1.68E-01	1.59E-02	-6.26E-03	1.16E-06	-1.82E-01	-4.48E-03	1.13E-01	3.20E-03	-2.37E-02	-2.56E-05	1.21E-05	1.36E-01	3.43E-03
220.0	-1.31E-01	9.27E-03	-4.39E-03	3.54E-06	-1.38E-01	-2.28E-03	2.24E-01	-2.07E-03	-1.21E-02	9.64E-06	-1.65E-06	2.43E-01	4.58E-03
240.0	-3.46E-02	4.82E-03	-2.50E-03	-6.05E-08	-3.73E-02	-4.34E-04	2.77E-01	-2.94E-03	-6.33E-03	7.11E-06	6.67E-08	2.90E-01	4.54E-03
260.0	6.58E-02	3.78E-03	-2.06E-03	2.93E-06	6.17E-02	-2.31E-03	2.67E-01	-3.89E-03	-5.96E-03	7.36E-06	7.41E-07	2.76E-01	-5.13E-04
300.0	9.56E-02	2.41E-03	-1.25E-03	-1.71E-07	9.96E-02	5.17E-03	2.04E-01	-3.33E-03	-5.46E-03	4.01E-06	4.05E-07	2.19E-01	6.03E-03
340.0	8.93E-02	7.52E-04	-3.10E-04	-1.48E-06	9.49E-02	6.01E-03	1.53E-01	-1.24E-03	-2.76E-03	4.67E-07	7.03E-09	1.61E-01	4.49E-03
380.0	5.30E-02	2.30E-04	-5.49E-05	-8.51E-07	5.64E-02	3.58E-03	1.13E-01	-3.65E-04	-1.43E-03	4.20E-08	-9.45E-09	1.17E-01	2.21E-03
420.0	-1.67E-03	8.32E-05	-4.77E-06	-8.21E-09	-1.38E-04	1.61E-03	8.74E-02	-7.00E-05	-8.10E-04	2.91E-09	-1.55E-09	8.91E-02	9.15E-04
460.0	-6.89E-02	5.55E-05	-1.86E-06	-2.86E-08	-6.82E-02	7.28E-04	7.57E-02	3.47E-05	-6.58E-04	-9.63E-10	6.28E-10	7.64E-02	5.07E-05
520.0	-1.91E-01	4.89E-05	-8.92E-06	-3.30E-08	-1.91E-01	3.55E-06	8.86E-02	8.92E-05	-5.24E-04	-2.18E-09	1.07E-09	8.90E-02	-1.45E-05
580.0	-3.23E-01	4.42E-05	-1.54E-05	-2.14E-08	-3.23E-01	-5.94E-06	1.29E-01	9.36E-05	-3.62E-04	-2.07E-09	5.16E-10	1.29E-01	-1.11E-05
660.0	-5.16E-01	4.13E-05	-1.90E-05	-1.21E-08	-5.09E-01	7.21E-03	2.27E-01	8.17E-05	-2.48E-04	-1.69E-09	1.08E-10	2.25E-01	-2.40E-03
750.0	-7.79E-01	3.22E-05	-1.63E-05	-4.85E-09	-7.28E-01	5.10E-02	4.19E-01	5.70E-05	-1.47E-04	-9.19E-10	-6.75E-11	3.92E-01	-2.66E-02

Table 9. Numerical values at 0.°0 latitude and 14.^{h}0 LST of terms in the momentum equations (11) and (12). Column headings are defined in Table 4.

ALTITUDE, KM (1)	(2)	(3)	(4)	(5)	(6)	(7)	(8)	(9)	(10)	(11)	(12)	(13)
125.0												
-7.70E-09	-0.	-2.69E-10	5.35E-11	-7.38E-09	1.00E-10	8.71E-02	0.	6.22E-02	0.	3.49E-19	2.29E-02	-2.04E-03
140.0												
-6.65E-08	-0.	-3.31E-09	-3.90E-10	-6.37E-08	-9.12E-10	1.41E-01	0.	1.24E-01	0.	1.22E-17	2.11E-02	4.40E-03
160.0												
-1.20E-07	-0.	-1.98E-09	-1.33E-10	-1.18E-07	-2.11E-10	6.53E-02	0.	6.23E-02	0.	3.79E-19	6.67E-03	3.71E-03
180.0												
-2.22E-07	-0.	-1.18E-09	9.59E-11	-2.22E-07	-1.52E-09	2.78E-02	0.	5.63E-02	0.	2.79E-18	-2.81E-02	3.75E-04
200.0												
-2.46E-07	-0.	-3.63E-10	3.95E-11	-2.47E-07	-1.38E-09	-3.12E-02	0.	3.07E-02	0.	1.48E-18	-6.31E-02	-1.16E-03
220.0												
-2.72E-07	-0.	-5.38E-11	1.49E-11	-2.73E-07	-1.30E-09	-8.07E-02	0.	1.70E-02	0.	6.89E-19	-9.95E-02	-1.87E-03
240.0												
-3.01E-07	-0.	4.98E-11	5.96E-12	-3.03E-07	-1.28E-09	-9.89E-02	0.	1.04E-02	0.	3.15E-19	-1.11E-01	-1.96E-03
260.0												
-3.37E-07	-0.	1.11E-10	9.81E-12	-3.35E-07	2.70E-09	-7.47E-02	0.	1.26E-02	0.	6.31E-19	-8.82E-02	-9.63E-04
300.0												
-1.17E-06	-0.	5.53E-10	3.10E-11	-1.18E-06	-6.63E-09	1.31E-04	0.	1.50E-02	0.	5.06E-18	-1.62E-02	-1.34E-03
340.0												
-1.39E-06	-0.	2.06E-10	9.94E-12	-1.40E-06	-9.87E-09	6.08E-02	0.	8.37E-03	0.	1.32E-18	5.29E-02	4.83E-04
380.0												
-1.40E-06	-0.	3.19E-11	2.87E-12	-1.40E-06	-8.45E-09	1.08E-01	0.	4.92E-03	0.	2.58E-19	1.04E-01	1.54E-03
420.0												
-1.36E-06	-0.	-3.59E-11	9.02E-13	-1.37E-06	-6.37E-09	1.38E-01	0.	3.01E-03	0.	4.43E-20	1.36E-01	1.63E-03
460.0												
-1.34E-06	-0.	-9.32E-11	6.36E-13	-1.34E-06	3.88E-10	1.55E-01	0.	2.57E-03	0.	7.73E-21	1.52E-01	1.74E-04
520.0												
-2.46E-06	-0.	-2.14E-10	6.72E-13	-2.47E-06	-6.19E-09	1.64E-01	0.	2.08E-03	0.	-3.57E-20	1.63E-01	1.21E-03
580.0												
-2.60E-06	-0.	-1.91E-10	3.18E-13	-2.60E-06	-1.30E-09	1.68E-01	0.	1.43E-03	0.	-2.82E-20	1.67E-01	2.96E-04
660.0												
-3.89E-06	-0.	-1.54E-10	1.84E-13	-3.89E-06	3.50E-09	1.80E-01	0.	9.34E-04	0.	-1.92E-20	1.78E-01	-4.54E-04
750.0												
-5.69E-06	-0.	-8.62E-11	8.94E-14	-5.67E-06	2.27E-08	1.93E-01	0.	5.01E-04	0.	-4.40E-21	1.88E-01	-3.96E-03

Geisler (1966) uses as his basic equation (in our notation)

$$2 \cos \theta \, v_\phi = \frac{1}{\rho r^2 \omega^2} \frac{\partial p}{\partial \theta} ,$$

$$- 2 \cos \theta \, v_\theta = \frac{1}{\rho r^2 \omega^2 \sin \theta} \frac{\partial p}{\partial \phi} . \qquad (14)$$

His atmospheric model, which is held fixed, is such that the right side of equations (14) increases nearly linearly with altitude. He therefore attributes this behavior to the velocities on the left side of equations (14). Later in his analysis he inserts the viscous shear terms as a correction, but these involve a second derivative with respect to altitude. Since the velocities are already determined to be nearly linear, this second derivative apparently reduces the contribution of the viscous terms to a very small magnitude, despite the large kinematic viscosity.

In a later paper Geisler (1967) improves the mathematical analysis; his formulation is quite similar to that of Kohl and King (1967). These authors solve an initial value problem with a diurnally periodic pressure gradient as a forcing function. They arrive at a final result when the wind system becomes diurnally periodic.

On the other hand, our analysis is a steady-state approach in which we look for a global equilibrium distribution of temperature, density, and wind velocity. This global picture automatically includes the diurnal effect; time derivatives are replaced by derivatives with respect to the longitudinal coordinate.

Although there is this basic difference between our approach and that of the other authors, it is not clear that this difference is sufficient to account for our disparate results: we find velocities that become negligible with increasing altitude, whereas they find velocities that increase to hundreds of meters per second with altitude. One possible reason for the different

results could be related to the numerical treatment of the basic equations. In our analysis the terms appearing in equations (13) are the most important ones at higher altitudes, while Geisler and Kohl and King may treat the terms in equations (14) or some other equivalent terms as the most important. We tried several different formulations and numerical-difference schemes, all of which led to the same result: the viscous and pressure-gradient terms are the most important.

Another possible reason for the different results is that our basic atmosphere is computed as a whole by means of the conservation equations. It has an inner consistency. Geisler and Kohl and King generate an empirical atmosphere based on simple algebraic and trigonometric formulas. Perhaps gradients over these empirical formulas do not properly describe the true situation. This reasoning must be recognized as conjecture on our part since these authors do not describe their analytical numerical techniques in detail.

One further point must be made. Any theoretical result, including ours, based on continuum fluid-dynamic equations above the altitude of 400 or 500 km must be taken con grano salis. At these altitudes the mean free path for particles is approximately equal to or greater than the scale height, and the problem moves into the realm of kinetic theory.

At the lower altitudes, where we find the winds to be of greatest magnitude, the viscous and pressure-gradient terms are usually the most prominent. This, however, is not always true (Tables 5 to 9), and other terms of the momentum equation may be of greater importance. It is interesting to note that the nonlinear terms never seem to play an important role, and following Geisler (1966, 1967) and Kohl and King (1967), we might just as well have omitted them.

In short, we find in our calculations that the wind magnitudes are greatest at the lowest altitudes, near 140 km, and decrease with increasing altitude. This behavior persists despite the fact that pressure gradients

sometimes increase with increasing altitude. The reason for this is the exponential increase of the kinematic viscosity with altitude.

At any given altitude, daytime winds away from the bulge are of greater magnitude than nighttime winds because daytime pressure gradients are steeper at higher latitudes.

At the lowest altitudes, near 160 km, the transport from the daytime to the nightime side is mostly in the east-west direction. At higher altitudes this transport is mostly over the poles.

4.2.2 Further comments on wind calculations

Kohl and King (1967), Geisler (1966, 1967), Challinor (1968, 1969), and we agree regarding the direction of the winds at any given altitude, that is, away from the daytime maximum and toward the nighttime minimum. None of these analyses shows a steady eastward wind of order 100 m/sec as predicted by King-Hele (1964). All these analyses, however, are based on equinoctial atmospheric conditions. Unfortunately, in considering solstice conditions, Geisler (1967) uses an atmospheric model that is essentially symmetric with respect to the equator. This model is revised by Jacchia and Slowey (1968), who show that there is a definite migration of the bulge with the subsolar point (in agreement with the theoretical results of Friedman, 1967). There has been no analysis of winds in the upper atmosphere with a truly nonsymmetric atmospheric configuration. Our formulation can easily handle such a problem and, if funding is available, we hope to work on it in the near future.

One further point must be made. All the above analyses have a common fault: They consider only winds on a horizontal surface and find for each surface a daytime source and a nighttime sink for mass flow. For these findings to be accommodated in a physically realistic manner, vertical winds must be introduced to feed mass into the source and to carry it away from the sink. In the next section we show that our computed winds cause a slight

density increase at higher latitudes and on the nighttime side of the earth. The physical consequence of this is that the atmosphere is taken out of hydrostatic equilibrium and vertical motions are induced. These vertical winds cannot be of large magnitude, and there is no provision in our present formulation for computing them. This is another problem for the future.

Papers by Rishbeth, Moffett, and Bailey (1969) and Dickinson and Geisler (1968) show that a vertical wind field of order 1 to 2 m/sec does exist and that it can have a measurable effect on the thermospheric energy balance. Both research teams worked with a fixed atmosphere and did not compute the effects of these winds on density profiles.

4.3 Effect of Winds on Density Profiles

We indicate by the dotted curves in Figures 3 to 5 the resulting density profiles obtained at altitudes of 300 km and above when density and winds are computed simultaneously. For this experiment we start with the same initial atmosphere as that used for the solid-line curves in the figures. Clearly, the difference in density between these two problems (wind and no wind) is small, the main reason being the small wind magnitude.

There is a slight decrease in density during the daytime at the equatorial latitude and a slight increase everywhere else — that is, there is a horizontal redistribution of mass so as to diminish the density and pressure gradients. This is to be expected on physical grounds. Furthermore, too great a transport of mass would not be expected at the various altitudes since this would bring the computed atmosphere out of agreement with the hydrostatic models, which have proved so successful.

In Figures 11 and 12 density profiles at altitudes between 125 and 200 km are shown. Here again the effect is small, especially at the higher latitudes. The main reason is that at these altitudes the viscous term is not always the dominant one in the momentum equations, the coriolis terms frequently becoming prominent. There is a complex interplay between these two forces.

When the coriolis terms are dominant, they match the pressure gradients, leading to geostrophic winds along the isobars. When viscous terms are dominant, which is the case at higher altitudes, the winds are across the isobars. The geostrophic winds are not so effective in moving mass and changing density distributions as are winds across the isobars.

Our computed wind fields have little effect on density. This implies that computing winds by use of a fixed density background (Geisler, 1966, 1967; Kohl and King, 1967) and not recomputing the densities will not lead to any gross errors. The fact that the wind does not greatly affect the density distribution could have been anticipated. One-dimensional models such as Jacchia's (1965) do not take into account any horizontal mass transport or wind, and yet these models give quite good results.

5. REFERENCES

BIRD, R. B., STEWART, W. E., and LIGHTFOOT, E. N.

1966. Transport Phenomena. John Wiley & Sons, Inc., New York, 780 pp.

CHALLINOR, R. A.

1968. The apparent rotation of the upper atmosphere. Planet. Space Sci., vol. 16, pp. 557-566.

1969. Neutral-air winds in the ionospheric F-region for an asymmetric global pressure system. Planet. Space Sci., vol. 17, pp. 1097-1106.

CHAPMAN, S., and COWLING, T. G.

1960. The Mathematical Theory of Non-Uniform Gases. Cambridge University Press, London, 431 pp.

CIRA

1965. COSPAR International Reference Atmosphere. North-Holland Publ. Co., Amsterdam, 313 pp.

COLEGROVE, F. D., JOHNSON, F. S., and HANSON, W. B.

1966. Atmospheric composition in the lower thermosphere. Journ. Geophys. Res., vol. 71, pp. 2227-2236.

DICKINSON, R. E., and GEISLER, J. E.

1968. Vertical motion field in the middle thermosphere from satellite drag densities. Monthly Weather Review, vol. 96, pp. 606-616.

FRIEDMAN, M. P.

1967. A three-dimensional model of the upper atmosphere. Smithsonian Astrophys. Obs. Spec. Rep. No. 250, 113 pp.

GEISLER, J. E.

1966. Atmospheric winds in the middle latitude F-region. Journ. Atmos. Terr. Phys., vol. 28, pp. 703-720.

1967. A numerical study of the wind system in the middle thermosphere. Journ. Atmos. Terr. Phys., vol. 29, pp. 1469-1482.

HIRSCHFELDER, J. O., CURTISS, C. F., and BIRD, R. B.

1964. Molecular Theory of Gases and Liquids. John Wiley & Sons, Inc., New York, 1249 pp.

JACCHIA, L. G.

1965. Static diffusion models of the upper atmosphere with empirical temperature profiles. Smithsonian Contr. Astrophys., vol. 8, no. 9, pp. 215-257.

1969. The neutral atmosphere above 200 km: a progress report. In Space Research IX, ed. by K. S. W. Champion, P. A. Smith, and R. L. Smith-Rose, North-Holland Publ. Co., Amsterdam, pp. 478-486.

JACCHIA, L. G., and SLOWEY, J. W.

1968. Diurnal and seasonal latitudinal variations in the upper atmosphere. Planet. Space Sci., vol. 16, pp. 509-524.

KING-HELE, D. G.

1964. The rotational speed of the upper atmosphere, determined from changes in satellite orbits. Planet. Space Sci., vol. 12, pp. 835-853.

KING-HELE, D. G., and HINGSTON, J.

1967. Variations in air density at heights near 150 km, from the orbit of the satellite 1966-101G. Planet. Space Sci., vol. 15, pp. 1883-1893.

KING-HELE, D. G., and WALKER, D. M. C.

1969. Air density at heights between 130 and 160 km, from analysis of the orbit of 1968-59B. Planet. Space Sci., vol. 17, pp. 985-997.

KOHL, H., and KING, J. W.

1967. Atmospheric winds between 100 and 700 km and their effects on the ionosphere. Journ. Atmos. Terr. Phys., vol. 29, pp. 1045-1062.

RISHBETH, H., MOFFETT, R. J., and BAILEY, G. J.

1969. Continuity of air motion in the mid-latitude thermosphere. Journ. Atmos. Terr. Phys., vol. 31, pp. 1035-1047.

SHIMAZAKI, T.

1968. Dynamic effects on height distributions of neutral constituents in the earth's upper atmosphere: a calculation of atmospheric model between 70 km and 500 km. Journ. Atmos. Terr. Phys., vol. 30, pp. 1279-1292.

WEIDNER, D. K., and SWENSON, G. R.

1969. Diurnal variations in the thermosphere from a series of Marshall — University-of-Michigan probes. Journ. Geophys. Res., vol. 74, pp. 4755-4764.

BIOGRAPHICAL NOTE

MANFRED P. FRIEDMAN received his B. Ch. E., M. S., and Ph. D. degrees from New York University in 1951, 1953, and 1961, respectively.

Before joining SAO in 1965, Dr. Friedman was a Research Associate in fluid dynamics at the Aerophysics Laboratory at Massachusetts Institute of Technology.

His investigations at SAO include theoretical studies of the upper atmosphere and the development of a method to describe the structure of the upper atmosphere.

NOTICE

This series of Special Reports was instituted under the supervision of Dr. F. L. Whipple, Director of the Astrophysical Observatory of the Smithsonian Institution, shortly after the launching of the first artificial earth satellite on October 4, 1957. Contributions come from the Staff of the Observatory.

First issued to ensure the immediate dissemination of data for satellite tracking, the reports have continued to provide a rapid distribution of catalogs of satellite observations, orbital information, and preliminary results of data analyses prior to formal publication in the appropriate journals. The Reports are also used extensively for the rapid publication of preliminary or special results in other fields of astrophysics.

The Reports are regularly distributed to all institutions participating in the U. S. space research program and to individual scientists who request them from the Publications Division, Distribution Section, Smithsonian Astrophysical Observatory, Cambridge, Massachusetts 02138.